What can be learned from natural analogue studies in view of CO2 leakage issues in Carbon Capture and Storage applications? Geochemical case study of Sainte-Marguerite area (French Massif Central)

Frédérick Gal, Michel Brach, Gilles Braibant, Claire Bény, Karine Michel

What can be learned from natural analogues studies in view of CO_2 leakage issues in Carbon Capture and Storage applications? Geochemical case study of Sainte-Marguerite area (French Massif Central).

GAL Frédérick, BRACH Michel, BRAIBANT Gilles, MICHEL Karine, BENY Claire

BRGM (Bureau de Recherches Géologiques et Minières)
Metrology, Monitoring and Analyses Division
3 Avenue C. Guillemin
BP36009
45060 Orléans cedex 1, France

Phone : + 33 (0)2 38 64 38 86
Fax: + 33 (0)2 38 64 37 11

E-mail : f.gal@brgm.fr

Abstract

Natural analogues studies have received much interest over past years through the CO_2 capture and storage applications. In this paper we focus on one natural analogue in leakage situation in order to describe the nature of the gas leakage, its interaction with surrounding rocks and aquifers and its behaviour over time. Soil gas and water monitoring techniques are used to gather point and continuous records. Leakage occurs along discrete sections relying on the nature of surface formations and the permeability of discontinuities. Main gas vents are perennial, relative proportions of different gas phases (CO_2, ^{222}Rn and ^{4}He) being dependent from the interaction with surface deposits and the distance to main tectonic pathways.

Mineral waters were also monitored as they represent integrative bodies that exist above nearly all CCS sites. Constraints on chemical processes occurring at depth are brought by characterisation of the dissolved constituents and by related isotopic systematics. Such determination of mixing processes and their influence is important, as leakage from CCS site may be evidenced through the mixing of the water from the storage complex and overlying aquifers. Longer term monitoring was conducted for physico-chemical parameters highlighting noticeable variations for pH, dissolved oxygen, redox potential and dissolved CO_2.

Keywords

Natural analogue

Carbon Capture and Storage

Soil gas monitoring

Water monitoring

1. Introduction

Natural analogues studies have received much interest over past years through the prism of CO_2 capture and storage (CCS) applications. Several references on this topic may be found in very recent papers such as *e.g.* Schütze *et al.* (2012). Natural analogues can either be in steady state conditions, *i.e.* in a non-leaking state, or at the opposite they can experience more or less developed leakages. In this paper we choose to focus on this second situation in order to evaluate how valuable information may be learnt from natural CO_2 leakages and extrapolated to CCS sites. In this particular case of leaking analogues, features devoted to the study of storage integrity are by definition unrealistic. Nevertheless, such analogues represent a good opportunity to illustrate what must be avoided for CCS sites (Bachu, 2003).

Even if vertical gas flows are often much greater than those expected in case of undesired CO_2 leakage from CCS site, natural analogues provide the opportunity to study the nature of a gas leakage, its interaction with surrounding rocks and aquifers, its behaviour over time or its potential impacts on surface environments (Lewicki *et al.*, 2007). Consequently, natural analogues monitoring is an appropriate way to study natural seepages and is from the authors' point of view complementary with induced leak experiments such as the ZERT (Spangler, 2010) or the CO2FieldLab ones (http://www.sintef.no/Projectweb/co2fieldlab/).

The Sainte-Marguerite site allows the study of both CO_2 leakage in shallow aquifers and gas escapes in near surface environments. Apart from pressure and temperature consideration, leakage in aquifers is the most critical parameter to assess for ensuring of CCS sites integrity. One must be confident with near surface monitoring technologies prior to use them in deeper environments. Second, monitoring of CO_2 escapes as a gas phase may consist in the ultimate warner prior to leakage in the atmosphere. Health and risk assessment and public acceptance directly rely on those two aspects.

Another interesting parameter to evaluate is the behaviour of natural analogues over long time periods. CO_2 injection is a very recent process compared to timescale of geological processes. Consequently, apart from failures linked to defective constraint of a CCS site (leakage due to abandoned wells, existence of fractures or leakage through the caprock; Lemieux, 2011), leakage may occur at low rate over years and may not be highlighted by monitoring technologies at depth, especially geochemical ones that rely on discrete measurements. A better understanding of how the gas migrates from depth and how it imprints surface environments is a challenging question that may be addressed by studying naturally leaking sites. Defining the origin of the gas phase is an important issue in case of leakage at a CCS site, helping to decipher whether the gas originates from the reservoir itself or from other sources that do not involve CCS processes (*e.g.* Gilfillan *et al.*, 2011).

The Sainte-Marguerite area belongs to the French Massif Central and more precisely to the southern part of the Limagne d'Allier basin (Figure 1). This tertiary basin is mainly filled by limestones with frequent sandy-clayey intercalations that are contemporary of the Oligocene to Miocene West European rifting. Alluvial and colluvial deposits from the Allier River partly overlie these tertiary strata and from place to place volcanic series crosscut the sedimentary formations. Mineral waters emerging in the Limagne d'Allier basin are strongly influenced by their deep circulation in the crystalline basement and the occurrence of deep CO_2 sources (Fouillac, 1983). The main tectonic structures, inherited from the Hercynian orogeny, are respectively N10-N30 and N110-N130 (Merle and Michon, 2001). The Sainte-Marguerite area is also characterised by the presence of travertine deposits formed from water degassing at springs (Casanova *et al.*, 1999; Fouillac, 1983; Rihs *et al.*, 2000).

While studies on mineral waters – mostly of sodium bicarbonate type with CO_2 present as a gas phase – from the Allier River valley are numerous (*e.g.* Négrel *et al.*, 1997a and

91 references therein), initial investigations of soil gas composition in the Sainte-Marguerite area
92 were performed during the 90's to locate new boreholes for perpetuating the commercial
93 exploitation of this water (Appora-Gnekindy, 1992; Baubron *et al.*, 1992). Earlier
94 measurements were made in the 70's on the west bank of the Allier River at the Saladis spring
95 (Batard *et al.*, 1978).
96 The objective of this study is therefore, in light of the work done in the 90's, to compare the
97 similarities and differences of gas emanations separated by 20 years. Point measurements and
98 longer records will be used to examine the relationships existing between the near surface
99 compartment and deeper seated processes.
100
101 Figure 1
102
103 **2. Methods**
104 Two types of investigative methods were used: soil gas characterisation and description of
105 water flows. Soil gas measurements were made using procedures and equipment identical to
106 those described by the authors elsewhere (*e.g.* Battani et al., 2010; Gal and Gadalia, 2011).
107 The monitoring methodology was based on the following:
108 - CO_2, O_2 and CH_4 soil gas concentrations were directly quantified in the field using
109 landfill gas analyser (LFG20 gas analyser, ADC Gas Analysis Limited, UK). Gas
110 content was measured at 1 m depth in order to minimize the effect of atmospheric
111 gases. CO_2 and CH_4 contents were determined by non-dispersive infrared absorption
112 and O_2 contents by electrochemistry. No CH_4 was found during the successive surveys
113 indicating concentrations lesser than 0.01% volume in the gas phase. As the CO_2
114 concentrations ranged from less than 1% up to 100%, precision of the measurements

varied between ±0.5% of the reading for CO_2 < 10% to ±5% of the reading for CO_2 > 50%.

- ^{4}He and ^{222}Rn concentrations were also systematically determined using samples collected in Tedlar bags for ^{4}He and vacuumed scintillating flasks for ^{222}Rn, respectively. Concentrations were obtained using mass spectrometry for ^{4}He (Adixen ASM102S leak detector, France) and scintillation counting for ^{222}Rn (Calen, Algade, France).
- Some additional grab samples were collected for laboratory determination of the $\delta^{13}C$ of the CO_2. The isotopic ratio was determined using a Delta S Thermo/Finnigan mass spectrometer and expressed as ‰ VPDB (Vienna Pee Dee Belemnite). A Varian 3400 gas chromatography was used for the determination of N_2, Ar, O_2, CO_2 and C_nH_{2n+2} (n = 1 to 6).
- Continuous data acquisition was also performed on ^{222}Rn content using Barasol probes (absorption spectrometry via a silicon detector; Algade) for long-term acquisitions (from October 2008 to March 2010). Barasol probes were protected by a PVC tube, covered by a Goretex membrane and buried at 1 m depth in the ground.

The joint determination of these gaseous species allow to compare information from tracers that may be enriched through geothermal reservoir processes (^{4}He), from poorly mobile elements that may help highlight areas with significant gas fluxes (^{222}Rn) and from a widely existing gas (CO_2) that may be tracer of soil/atmosphere exchanges or of deep seated endogenic processes. Weather conditions were also taken into account for the interpretation of the soil gas data and will be discussed together with the data.

Secondly, as the Sainte-Marguerite area is known for its mineral water resources, chemical characterisation of some springs (physico-chemical parameters and dissolved ions content) was also performed as well as the monitoring of the Brissac Geyser during several hours using a multi-parameter Idronaut probe (Idro316*Plus*). Dissolved ion contents were determined at laboratory using ICP-AES (Inductively Coupled Plasma – Atomic Emission Spectroscopy) and chromatographic methods. Isotope ratios were measured by gas phase mass spectrometry ($\delta^{18}O$ and δD are expressed in ‰ VSMOW – Vienna Standard Mean Oceanic Water). The Idronaut probe was used to monitor the short-time evolution of temperature, pH, specific conductance, dissolved oxygen, redox potential and dissolved CO_2 content of the water.

3. Gas and water measurements

3.1 Soil gas data

A dataset of nearly 1000 data points for each gas specie (CO_2, ^{222}Rn and ^{4}He) is available, half of them from the 90's measurements and the rest from more recent measurements (Table 1).

Table 1

CO_2 concentrations range from values close to those of the atmosphere up to 100% vol. The frequency distributions are different between the two measurement periods in relation to the spatial arrangement of the measurements that is dictated by the tectonic and geological structure of the study area. As a consequence, the mean CO_2 concentration is significantly greater for the 2006-2010 dataset than for the 1992 dataset.

Radon-222 (^{222}Rn) concentrations also fall within similar ranges during the two periods, minimum values being close to 150 $Bq.m^{-3}$ and greater ones around $2x10^{6}$ $Bq.m^{-3}$. The mean

values were again higher for the 2006-2010 period as a consequence of data acquisition mainly focused on the Western part of the area. Nevertheless the variation of mean concentrations is only a factor of two whereas it was a factor of four for CO_2 concentrations. Helium-4 (^4He) concentrations are on average quite close to the atmospheric content but this value hides important differences. Both in 1992 and 2006-2010 some measurements showed very strong depletions when compared to the atmospheric content while others had strong enrichments ($\geq$ 10 ppm).

Most of the CO_2 measurements made between 2006 and 2010 were also supplemented by measurements of the O_2 concentrations in soils. A very homogeneous inverse behaviour exists between those species (Figure 2). Almost all data exhibit an O_2 decrease that is not proportional with the increase of the CO_2 content on a per mole basis. Depletion of O_2 is much faster with a factor close to 5. This suggests that CO_2 is supplied in abundance by a powerful process probably related to a deep gas source (crustal and/or mantle origin) as will be discussed later.

Figure 2

This strong O_2 depletion is also confirmed by the gas chromatography measurements reported in Figure 3. Correlations with other gas species follow linear regression with r^2 between 0.991 and 0.998, and also suggest a different behaviour between the CO_2 end-member and the N_2-O_2-Ar triptych, with CO_2 becoming predominant as the other three gases diminish and vice-versa. This was particularly true for a 30 m deep borehole where atmospheric constituents were only detected at trace levels (0.13% N_2; 0.023% O_2; 0.002% Ar). Using the relationship presented in Figure 3, it is then possible to recalculate an average composition for the

189 atmospheric end-member. Ar and N_2 contents were respectively at 0.932% and 79.6%, levels
190 that are very close to those usually reported for the atmosphere (respectively 0.934 and
191 78.08%; http://encyclopedia.airliquide.com/). Unlike O_2, which is subject to a more active
192 kinetic of replacement, N_2 and Ar are diluted in the soil gas by equimolar replacement with
193 CO_2.
194
195 Figure 3
196
197 Finally, the $\delta^{13}C$ isotope ratio of the CO_2 gas was also evaluated on these samples and ranged
198 between -3 to -5.1‰ VPDB for CO_2 in the 14 – 100% vol. range.
199
200
201 3.2 Water measurements
202 The main physico-chemical properties of mineral springs sampled during the study are listed
203 in Table 2. A rain event collected in October 2008 is also reported for comparison. The
204 emergence temperatures range between 16 and 30°C and pH between 6.2 and 7.2, therefore
205 comparable to those reported by Négrel *et al.* (1997b) for the carbogaseous waters known
206 throughout the French Massif Central. Specific conductances vary between 2.5 and 8.4
207 $mS.cm^{-1}$, Chapelle springs (used for bottling) having total mineralization approximately half
208 of other sampled waters. The mineralization is dominated by HCO_3 (1.3 to 4 $g.L^{-1}$), Na (0.3 to
209 1.5 $g.L^{-1}$) and Cl (0.2 to 1.5 $g.L^{-1}$). If this Na-Cl-HCO_3 facies predominates, the Ca and Mg
210 amounts, less variable (respectively 120 to 310 $mg.L^{-1}$ and 100 to 140 $mg.L^{-1}$), allow the
211 Chapelle springs – due to their lower dissolved elements concentrations – to be linked with
212 the Ca-Mg pole, suggesting a secondary enrichment associated with the chemical hardness of
213 bicarbonate-rich waters (Michard *et al.*, 1981). Similarly, the Chapelle springs have an

214 oxidizing character contrary to Tennis and Geyser Brissac waters that are characterized by a
215 marked reducing character. Characteristics of isotope ratios reported in Table 2 will be
216 discussed in section 5.
217
218 Table 2
219
220
221 **4. Interpretation of soil gas data**
222 4.1 Point data
223 One of the first steps to considered for highlighting a potential leakage at a CCS site is to
224 characterise the CO_2 phase. Concentration measurements are of great interest but they may
225 not be sufficient *e.g.* in case of small leakage rate. Additional information may be gathered
226 using isotope systematics, mobile systems nowadays allowing on-site measurements (e.g.
227 Picarro or Aerodyne lasers). $\delta^{13}C$ isotope ratio measurements will not give direct indication of
228 the process that may be involved in the production of the CO_2 phase but will allow 1) to
229 discriminate between several origins and 2) to discard some unrealistic origins.
230 In the case of Sainte-Marguerite, CO_2 concentrations in soils are supposed to evolve primarily
231 under the influence of deep seated processes rather than surface processes. Indeed, the range
232 of $\delta^{13}C_{CO2}$ isotope ratios in soil gas (-3 to -5.1‰) is related to deep crustal and/or mantle
233 degassing (-4 to -8‰; Gerlach and Taylor, 1990). Similarly, $\delta^{13}C_{CO2}$ are close to ratios
234 measured on the gaseous phase of low helium concentrated, CO_2-rich waters from the Massif
235 Central (-6.4‰; Dégranges *et al.*, 1978). The more depleted ratio (-5.1‰) was measured in
236 the 30 m borehole, where the gas phase was 100% CO_2 with no ^4He (< 0.05 ppm), whereas
237 soil gas measurements (1 m depth) were slightly enriched in carbon-13 (*i.e.* greater than -
238 4.8‰). This slight isotopic enrichment of upper soil horizons may be the result of two

239 complementary phenomena, first the percolation of CO_2 through surface aquifers ($\delta^{13}C$ of
240 dissolved carbon from local springs close to 10.2‰; Mercier, 1987) and second the
241 interaction with travertine deposits ($\delta^{13}C$ between 5.4 and 7.7‰; Casanova *et al.*, 1999).
242
243 In the case of leakage originated from a CCS site, such characterisation using the only $\delta^{13}C$
244 isotope ratio will be much more difficult as overlaps between several gas origins and frequent
245 re-equilibration will certainly occur. A way to better constrain gas emanation is to measure
246 other gas species with different chemical properties.
247 In the present study we mainly refer to ^{222}Rn and ^{4}He. As ^{222}Rn and ^{4}He are only present as
248 trace levels in the free atmosphere (respectively around 50 $Bq.m^{-3}$ or less and 5.24 ppm), an
249 enrichment would favour the existence of phenomena occurring either in the soil or in the
250 upper regolith (^{222}Rn) or deeper in the ground (^{4}He; Battani *et al.*, 2010; Gilfillan *et al.*, 2011).
251 Relationships between CO_2, ^{222}Rn and ^{4}He are presented in Figure 4.
252
253 Figure 4
254
255 For $^{222}Rn/CO_2$ and $^{4}He/CO_2$ couples, graphical relationships (Figure 4A) confirm the different
256 origin of these two gases and highlight that the genesis of ^{4}He from radioactive decay of
257 uranium in the near surface has little influence on the ^{4}He concentrations. This should also
258 result in an increase of the ^{4}He concentration when ^{222}Rn activities are high. This is not the
259 case, since there is rather a gradual depletion when the ^{222}Rn activities exceed 10^{6} $Bq.m^{-3}$
260 (Figure 4A). Moreover, these high ^{222}Rn concentrations are measured at precise locations
261 which correspond to surface discharges of springs (old factory and Tennis; Figure 1) that form
262 tens of centimetres to several meters thick travertine beds. These very high ^{222}Rn activities are
263 presumably related to these travertines, consequently richer in uranium than the alluvial

formations and the local waters (Casanova *et al.*, 1999). In this particular case, the CO_2 source is not strong enough to dilute the ^{222}Rn as may occur farther from travertine deposits. As a consequence, perennial ^{222}Rn high concentrations exist locally.

The behaviour of ^{222}Rn and CO_2 is also complex for ^{222}Rn concentrations lesser than 300,000 $Bq.m^{-3}$ (Figure 4B). Two distinct trends seem to exist, one with fast ^{222}Rn enrichment with low CO_2 concentrations (red squares), and the other with weaker ^{222}Rn enrichment when CO_2 concentrations rise (blue lozenges). These two behaviours correspond to various spatial locations (Figure 5). Most of the "high ^{222}Rn – low CO_2" samples plot on the eastern part of the site on sedimentary deposits (mean altitude 350 to 365 m), whereas the majority of the "low ^{222}Rn – high CO_2" group is restricted to a lower terrace of the Allier river (westward from longitude 669,100 in Figure 5 – mean altitude 335 to 345 m; see also Battani *et al.*, 2010 for geological cross-section). Near the Allier River, the thickness of geological formations overlying permeable paths is lesser than eastward. The CO_2 gas interacts to a lesser extent with surface formations, leading to moderate ^{222}Rn enrichment. On the contrary, on the eastern part of the site, CO_2 has to go through thicker formations (alluvial and Oligocene formations), leading to smaller CO_2 amounts and also to ^{222}Rn enrichment due to the percolation of the CO_2 into these formations. An intermediate behaviour occurs above travertines deposits (Figures 4 and 5) where the ^{222}Rn content is also dependent from the uranium content of these formations. An additional process can also act in a complementary fashion. Deep CO_2 may be less diluted on the western part of the site than on the eastern part, indicating a more pronounced upward flow that allows the dilution of radon signal (Baubron, 1992; Gal *et al.*, 2011).

No relationship can be highlighted for the $^{4}He/CO_2$ couple except from a very weak tendency of having slightly lower ^{4}He concentrations when CO_2 concentration is greater than 50% (Figure 4A). If considering the 30 m depth borehole as the most representative of the deep

289 end-member, then uprising gas flow is ^{4}He depleted. A strong CO_2 flux can act as a flushing
290 agent on ^{4}He. For lesser CO_2 amounts, flushing effect may be less important and ^{4}He
291 concentrations are higher or even enriched depending on the amounts of ^{4}He upward
292 migrating.
293
294 Figure 5
295
296 The great variability of soil gas concentrations on a small area is not only dependent from
297 deep processes but also from the heterogeneity of surface formations and pathways. Such a
298 problematic is critical for CCS sites especially in areas where potential leakage pathways are
299 not well characterised. This will raise the question on how detect surface leakage if *e.g.* a
300 leakage occurred in deep groundwaters. Nevertheless, a positive point is the persistence of
301 leakage structures over years.
302 As a result, the Sainte-Marguerite area presents a patchy repartition of anomalies at surface,
303 as evidenced by the equal concentration lines reported on Figure 6. Data are interpolated
304 using natural neighbour algorithm. This interpolation method is more rugged than *e.g.*
305 kriging, but it has the advantage in not extrapolating the contours beyond the convex hull of
306 the dataset. The whole dataset is presented top of Figure 6. Separate contributions from the
307 data acquired during the 90's and during the 2000's are respectively presented middle and
308 bottom parts of Figure 6. A good match is highlighted between these 15-year interval datasets
309 especially on the Western part of the study site where strong CO_2 enrichments remain
310 perennial. The match cannot be achieved for the Southern part as a new bottling facility has
311 been built in between time therefore no measurement is yet possible. The North-South to N10
312 anomalous zone is well in agreement with structural directions reported in the Limagne
313 d'Allier basin (Merle and Michon, 2001). This direction is also suggested by variogram

computations (data not shown) which suggest, under a spherical model, a significant nugget effect (40% of the variability) and a reduced leg (20 m). Consequently, there seems to be at site scale a structure directly related the Hercynian tectonic and at a smaller scale a less obvious structure that is difficult to model even with a large amount of data.

For CCS site management, this suggests that once fed by seepage or microseepage, a leakage pathway will remain active over a long time period. Its characterisation will then be possible but remediation actions will be very difficult to undertake.

Figure 6

The complex CO_2 distribution in soils is not restricted to this gas phase. A well characterised time coherence for ^{222}Rn concentrations (90's and 2000's datasets) also exists and reveals an anomalous area close to the flow axis of the Allier river (Figures 2 and 6). A N170 direction is suggested by variogram calculations, with a leg identical to that defined for CO_2 but with increased nugget effect (50% of the variability). This may be linked to the location of the area of maximum ^{222}Rn concentrations, close to the high CO_2 area but with no coinciding peaks, and due to the difference of origin for these two gases, radon being preferentially produced in shallower environments than CO_2 in the present case.

The evolution of ^{4}He concentrations in the area where ^{222}Rn and CO_2 anomalies are located is very interesting to detail (Figure 6). This area is characterized by a complex intricacy of positive and negative anomalies in helium *i.e.* tracing enrichment or depletion with respect to the atmospheric content. This complexity in ^{4}He emanations is remarkably stable over time. Low ^{4}He concentrations are preferentially measured along a N10 axis, locally reinforced by a

complementary N160 direction. The adjustment on a spherical model of the variogram suggests a maximum correlation distance of 40 m between two points without a nugget effect.

In order to better assess the behaviour of CO_2, ^{222}Rn and ^{4}He, a linearization of the data was made using the scheme proposed by Michel – Le Pierrès *et al.* (2010). The resulting interpolation map is presented in Figure 7. By assumption, CO_2 and ^{4}He are considered as deep end-members and ^{222}Rn as a near surface produced gas. This is consistent with gas origins suggested by Jeandel *et al.* (2010) that found a nearly half/half mantle/crust origin for helium and a predominant crustal origin for CO_2. This strengthens previous results indicating that CO_2 and ^{4}He amounts are not directly proportionally linked. The linearization process is then intended to lower the influence of ^{222}Rn and to over-estimate the one of ^{4}He by assigning a value between 0 and 1 to each of the gas specie. The 0.05 to 100% CO_2 range is restricted in the 0 – 1 interval and so on for ^{222}Rn (140 to 248,000 $Bq.m^{-3}$) and ^{4}He (0.05 to 9.83 ppm). Using this procedure, ^{4}He concentrations account for *c.a.* 75% of the total variability, CO_2 for 22% and ^{222}Rn for the rest (*c.a.* 3%). Despite this bias introduced in the dataset (Figure 7), the surface geometry of the anomalies is still primarily guided by the distribution of CO_2 concentrations, the influence of ^{4}He been of second order. Consequently, it is the deep CO_2 source that governs the spatial distribution of anomalies in soil gas through the N10-N30 and N110-N130 structures (Merle and Michon, 2001). Other gaseous species evolve either through the heterogeneous composition of the regolith or through the existence of complex phenomena including convective transport, stripping or mixing. This strong imprint of geological structures on the occurrence of anomalies also appears in the comparison of data acquired 15 years apart, since changes between these two periods remain small. This statement is strengthened by comparison with CO_2 flux data available in the area (Battani *et al.*, 2010). The most anomalous CO_2 areas correspond to those marked by fluxes reaching or

363 exceeding 500 $cm^3.min^{-1}.m^{-2}$, while the radon anomalies are superimposed on areas where the
364 fluxes are smaller (lesser than 100 $cm^3.min^{-1}.m^{-2}$).
365
366 Figure 7
367
368 4.2 Time evolution of soil gas concentrations
369 Evaluation of short-term variability of soil gas concentrations was evaluated using point
370 measurements (CO_2, ^{222}Rn and ^{4}He) and continuous measurements (on the CO_2 phase using
371 Fourier Transform Infrared gas spectrometry). Repeated point measurements over 3 days
372 (points 1 to 4 in Figure 1) indicated that the points located northward of the site experienced
373 low variability of their gas concentrations (± 60% for CO_2). At the opposite points located in
374 the southern part of the site had much greater variations rising up to a factor of 80 for CO_2 and
375 200 for ^{222}Rn (point 4). Continuous measurements in upper soil horizons in the vicinity of the
376 Brissac Geyser had an intermediate variation factor of 8 over few hours, with periodicity
377 influenced by the geyser own kinetic (mean period of 21 minutes).
378 Assessing the variability of gas emanations at short time scale is important for the
379 comprehension of phenomena occurring at a natural analogue, but such a time scale is not
380 fully matching requirements of CCS site monitoring. Longer chronicles shall be available in
381 order to highlight any deviation from environmental background noise. The Sainte-Marguerite
382 site has then been instrumented for longer-term measurements. They were performed only on
383 the ^{222}Rn phase for practical reasons. Even if deviations that may be recorded will not be
384 linked to deviations from an environmental background noise in the present case, one must be
385 confident in the capacity of monitoring devices to properly register unexpected events.

Points 2 and 4 (Figure 1) were instrumented with Barasol probes from October 2008 to January 2009 for hourly monitoring and afterwards only the point 4 remained. Soil temperature and barometric pressure were simultaneously recorded at 1 m depth in the soil. Meteorological data were got from an airport weather station located 14 km NNW from Sainte-Marguerite, at similar altitude. Two distinct time responses exist (Figure 8):

- Pressures measured at 1 m depth in soils perfectly replicate the variations of atmospheric pressure and provide accurate description of local evolutions (Figure 8a);
- Temperatures measured in the soil are different from those measured in the atmosphere (Figure 8b). Soil temperatures exhibit a smoother daily variability and are higher than atmospheric temperatures. There is a time-lag between the maxima of temperature in the atmosphere and in the soil, the former occurring 5 to 6 hours before the later.

In December 2008 and January 2009, there is however a difference between temperatures measured by the two probes (Figure 8b). The probe located in the southern part of the study area (point 4 in Figure 1) recorded higher temperatures (from 5 to 10°C) than those measured a few hundred meters northward (point 2 in Figure 1). Point 4 being located in a depression close to mineral springs (25 to 29°C at the orifice), this warming may be related to their influence into higher groundwater level during winter times.

Figure 8

Radon activities measured by the 2 probes during the October 2008 - January 2009 period showed trends with site-specific evolution but the variability of the measurement remained in a similar range (Figure 8c). There is a good agreement between average ^{222}Rn concentrations computed from Barasol records (Table 3) and that from point measurements performed at site

scale (Table 1). Marked activity peaks nevertheless occurred. At the end of January 2009 (Figure 8c), phenomenal concentrations were reached (up to $80x10^6$ $Bq.m^{-3}$). Such concentrations remain under saturation threshold of the probe (10^9 $Bq.m^{-3}$) but are far greater than maximum values found during spot sampling ($2.5x10^6$ $Bq.m^{-3}$). During this January 2009 event, a perfect synchronism was found between the 2 probes with a very quick increase followed by very small ^{222}Rn amounts few hours later. This event is therefore not related to malfunctioning of the equipment. The measurements suggest a gas burst sweeping the area of Sainte-Marguerite, leading to a huge increase in ^{222}Rn and a subsequent strong depletion. Concentrations remained low until radioactive decay produced again a sufficient amount of ^{222}Rn. Another peak of activity was also detected in September 2009 (Figure 8c). However, as only one sensor was deployed and as it experienced some operational problems, we prefer not trying to interpret this latter signal.

Table 3

Apart from these specific periods, the ^{222}Rn concentrations change cyclically (Figure 8). Cycle analysis returned variable results depending on the analysed time period and even on the location of the probe (Table 3). There was no clear influence of external forcing such as daily or diurnal variations over long time periods or the existence of pulsation of longer duration. It is therefore not possible to highlight regular gas emanations as may be possible regionally such as in the vicinity of Lake Pavin (Gal and Gadalia, 2011).

Nevertheless, during periods characterised by less noisy ^{222}Rn signals (March 2009; Figure 9a, b and c), a daily cyclicity (24 hours period) clearly appeared even if trends of greater wavelength may also contribute to the shape of the recorded signal (Figure 9d). Principal Component Analysis were calculated by combining the factors accounting for maximum

variability (Figures 9e and f). The only apparent trend was an inverse correlation between ^{222}Rn concentration and soil temperature. Given the interdependence between soil and atmospheric temperature, this trend can be extended to this second parameter. Thermal forcing seemed to be more efficient than pressure gradients to influence the short-term temporal evolution of ^{222}Rn concentrations, apart from sudden phenomena such as "gas bursts".

Figure 9

As previously described, the occurrence of large ^{222}Rn concentration peaks was very intriguing. The origin of such short pulses may typically be attributed to external causes such as earthquakes. Radon is frequently used as an indicator of crustal movement (precursor), although each earthquake does not raise an ^{222}Rn anomaly and each anomaly is not necessarily followed by an earthquake (*e.g.* Al-Hilal *et al.*, 1998). According to dislocation model (Fleischer, 1981; Fleischer and Mogro-Campero, 1985), variations of ^{222}Rn concentrations issued from stress changes can be detected even at great distances from epicentres, involving a wide set of mechanisms (Kharatian *et al.*, 2002). Continuous measurements of ^{222}Rn in soil gas sometimes allow the identification of spike-like anomalies just before the earthquake, the post-seismic stage being characterised by a rapid return to natural background values (Chyi *et al.*, 2002). Although highly variable, increases in ^{222}Rn concentrations at 1 m depth in soils (Wattananikorn *et al.*, 1998) often occur between 4 and 15 days before earthquakes of magnitude 2 to 6 with distances from the epicentre to the measuring station comprised between 15 to 250 km (Das *et al.*, 2006; Ghosh *et al.*, 2007; Ramola *et al.*, 2008).

Referring to these constraints, we searched the available databases (http://www-dase.cea.fr/) for events reported in an area covering 4 degrees in longitude and 3 degrees in latitude, centered on Sainte-Marguerite. Twelve earthquakes were recorded between January 28 (12 hours after the ^{222}Rn peak) and February 13 (17 days after the ^{222}Rn peak) within this area, at distances between 40 and 70 km from Sainte-Marguerite. All were characterised by very low magnitudes less than 2.5. Although some of the cited literature reports a sensitivity of ^{222}Rn measurements for low seismic magnitudes, no clear relationship exists in the present case between ^{222}Rn peaks and tectonic activity.

Such excursions of ^{222}Rn signal were earlier reported on the Weyburn site, which is not known to be tectonically active (Riding and Rochelle, 2009). Phenomena observed at Weyburn were short (3 hours) and activities varied by factors of 7 to 15. At Sainte-Marguerite variations were consequently higher (100 to 1000 times) and the sensitivity of ^{222}Rn concentrations to pressure changes was less obvious than stated at Weyburn. This renders improbable an origin related to transient phenomena affecting the pressure.

Even if not really successful during the monitoring period, long-term measurements of soil gas emanations are of strong interest in view of CCS applications. Data main not only be gathered on the ^{222}Rn phase but mostly on CO_2 and/or O_2 phases. This is crucial for assessing if variations are linked to natural processes, either originated from surface processes or deeper ones, or caused by CCS operations. Continuous monitoring is not designed to cover great areas, one limiting factor being costs, but is complementary with point techniques and may be deployed in most prominent locations highlighted by point monitoring.

5. Chemistry of mineral waters

The Sainte-Marguerite site offers the opportunity to monitor gas escapes into more or less mineralised water bodies. We will first describe water chemical compositions and then discuss what is important in view of long term water monitoring.

5.1 Point sampling

Mineralisation of these waters form two groups, one rich in dissolved constituents and belonging to the Na-Cl-HCO_3 end-member, the other (Chapelle springs) more influenced by the Ca and Mg species. This distinction remains when referring to $\delta^{18}O$ and δD isotope ratios (Table 2). Chapelle springs are always under the local meteoric water line (Fouillac *et al.*, 1991), *i.e.* enriched in heavy isotopes contrary to other springs which fall on this meteoric water line. This may be related to evaporation (Négrel *et al.*,1997b and references therein), to mixing in various proportions between deep and surface end-members (*e.g.* Michard *et al.*, 1981) or to mixing between different deep end-members (Négrel *et al.*, 1997b; Rihs *et al.*, 2000). These differences in isotope ratios denote spatial disparities within walking distance but do not imply the existence of compartmented geological structures. Theoretical calculations of the ^{13}C isotope signature of gas in equilibrium with the waters provide ratios between -2.8 and -5.1‰ (Table 2) that exactly match the range measured in soil gas. Water mixing must then occur under open system conditions allowing different end-members to interact one with each other, pro parte explaining temporal variations reported in the area (Négrel *et al.*, 1997b).

Strontium isotope ratio of water ($^{87}Sr/^{86}Sr$) is known to derive from that of minerals with which the water interacts and to be lower than that of the whole rock, in response to different dissolution rates between the mineral species (*e.g.* Michard *et al.*, 1978). $^{87}Sr/^{86}Sr$ ratios (Table 2) suggest that Tennis and Geyser Brissac waters fall in the range of ratios known across the Limagne d'Allier (0.71338; Stettler, 1977) and therefore reflect the signature of a

deep end-member. Lower ratios of Chapelle springs suggest either an interaction with lithologies different from those present in the supply circuit of Tennis and Geyser Brissac springs (*e.g.* plagioclase from the Coudes granite at 0.71028; Rihs *et al.*, 2000) or a mixing with near surface groundwaters (ratio close to 0.71102; Négrel *et al.*, 1997b). In the first case (mixture of 2 groundwaters, one coming from plagioclase weathering), a contribution of the deep end-member (represented by Geyser Brissac or Tennis springs) close to 32% can be calculated using a binary mixing law, whereas in the second case (dilution by surface water), the proportion of the deep end-member may be close to 57%.

Using this deep end-member – or at least the end-member less affected by mixtures – equilibrium temperatures with basement rocks may be evaluated referring to cationic geothermometers. As geothermometers induce the existence of equilibrium between waters and rocks, we neither refer to Ca and Mg geothermometers, strongly affected by mixing processes (Michard *et al.*, 1981), nor to silica -rich species, oversaturated with water at the spring orifice. Na/K (Michard, 1979, 1990, Truesdell, 1975) and Na/Li (Fouillac and Michard, 1981; Michard, 1990) geothermometers are preferred as saturation indices of mineral species containing Na indicate under saturation with water. Deep reservoir temperature is estimated between 180 and 210°C (Na/K) and 195 and 205°C (Na/Li). This estimate is in agreement with that of Fouillac and Michard (1981) and Fouillac (1983).

Isotope characterisation of waters is often restricted to the monitoring of ^{18}O, ^{2}H or ^{13}C species in view of CCS problematic. Such characterisation is important but water monitoring of deep aquifers, such as the storage complex itself of overlying aquifers, may include other species. O, H, C species may suffer from several processes such as water/rock interaction of mixing between different water bodies. Monitoring other isotopes, such as Sr, Nd, B, Li, Ca

533 or U may also allow getting information on deep seated processes, better define water/rock
534 interaction or describe redox processes. A better comprehension of deep phenomena may
535 allow improved constraint on CO_2 migration in deep horizons if leakage from the storage
536 reservoir may occur.
537
538 5.2 Continuous monitoring of Geyser Brissac
539 Here we describe short-term evolution of some key physico-chemical parameters of the
540 Geyser Brissac mineral water. Requirements of CCS monitoring will obviously not imply
541 high frequency measurements but one must be confident on the short time scale before
542 assessing variations of longer period.
543 Results of this monitoring are presented in Figure 10 and Table 4. Two days were
544 characterised by sunny conditions whereas rainfall events of variable magnitude occurred
545 during day 4 and especially day 3. The evolution of dissolved CO_2 is reported on Figure 10
546 even if quantification is not accurate using pH-based sensors (Gal *et al.*, 2011), in order to
547 bring qualitative information.
548
549 Figure 10
550 Table 4
551
552 A cyclical pattern is clearly apparent for all the parameters, directly related to Geyser Brissac
553 dynamics (Figure 10). Two parameters mainly influence the water temperature: 1) intrinsic
554 processes, the eruption of the geyser progressively warming the water and 2) atmospheric
555 forcing, higher water temperatures being recorded around 16:00 in the evening. This is due to
556 to the location of the Geyser Brissac, emplaced in a 1 m deep, 5 m diameter bowl filled with
557 mineral water. Measurements were performed at the bottom of this bowl, closest to the drain

where the geyser overflows. The presence of non-flowing waters induced the occurrence of thermal forcing on this water mass: time is needed for the water directly flowing from the geyser when it erupts to warm up the bowl. Similarly, amplitude of the temperature peaks becomes smaller through the day and the water mass becomes hotter as solar heats the water mass. Dilution effects due to rainfall may happen and significantly affect the water temperature and the specific conductance (day 3, Table 4).

Apart from external causes, time evolution of the records is dependent from the geyser activity. Temperature peaks, which correspond to the maximum of the activity of the geyser, lasted 4 to 5 minutes. They are synchronous to increase of the dissolved CO_2, slight decrease of the pH value (-0.05 pH unit) and decreases of the dissolved O_2 concentration and of the redox potential. Such evolutions are self-consistent and reflect the progressive replacement of O_2 by CO_2 in the bowl as the eruption takes place. Specific conductance is also affected, CO_2 inflows leading to harmonic variations of the record. Nevertheless, diurnal heating affects the dissolved CO_2 measurements, one of the drawbacks of this sensor elsewhere reported (Gal *et al.*, 2011).

Spectral density analysis is best constrained using dissolved O_2, pH and redox potential redox. Main period is around 22±1 minutes in good agreement with infrared measurements performed in soils (see section 4.2). As measurements were not conducted over several days, it is not possible to identify periodicity of greater wavelength such as that determined from Barasol probe acquisitions.

Long-term monitoring of water bodies is one of the key procedures in order to ensure of the safety of CO_2 storage. Monitoring performed at Sainte-Marguerite natural analogue shows that this method is sensitive to strong CO_2 leakage well over thresholds expected in deeper environments. Nevertheless devices have the capacity to record variations of lower

583 magnitude. The main issue nowadays existing relies on the stability of the sensors over time.
584 Long-term deployment at depth generally involves CTD probes, *i.e.* probes that measure only
585 temperature, specific conductance and depth. This only involves solid state sensors. Idronaut
586 probe has chemical sensors for all other parameters and such sensors are subject to drift.
587 Dissolved oxygen may be better constrained using optical sensors. Until now, no long-term
588 pH or redox monitoring has been reported without frequent recalibration of the devices. This
589 question is of crucial importance, as pH is one of the most sensitive parameter to monitor
590 changes linked to CO_2 dissolution.
591
592 **6. Concluding remarks**
593 This case study of Sainte-Marguerite natural analogue allows investigating both soil gas and
594 water compartments.
595 Point soil gas measurements have suggested the presence of perennial pathways that favour
596 gas escape from depth to the surface by comparing data acquired 15 years apart. Leakage does
597 not occur along all the fault length as may be derived from geological maps but rather along
598 discrete sections. At Sainte-Marguerite there is no visual impact on the vegetation as could
599 exist in other similar environments (Krüger *et al.*, 2011; Schütze *et al.*, 2012). Permeability of
600 faults does not exist as a whole mechanism but rather as narrow structures separated by less
601 permeable sections filled by secondary mineralization. In terms of CCS monitoring strategy,
602 this suggests that potential pathways that may be deduced from geological or geophysical
603 works may not be the most prone to become pathways. It would be better to search for
604 structures that are still open to fluid draining *i.e.* secondary fractures that are more likely to
605 have intrinsic permeability than main discontinuities.
606 The CO_2 gas was found to be the main carrier gas leading to the existence of gas anomalies in
607 near surface environments. Carbon isotope ratios are mainly imprinted from deep seated

608 processes with little interaction in near surface environments either resulting from percolation
609 into surface waters or into travertines horizons. Helium concentrations measured in CO_2-rich
610 areas also highlighted this strong imprint of crustal contribution (Jeandel *et al.*, 2010). The
611 interaction of fluids with travertine deposits also influenced the ^{222}Rn concentrations of the
612 gas phase. Consequently, gas emanations were found to be mainly oriented along known
613 regional directions of the tectonics with some complications induced by local surface geology.
614 When alluvial deposits were the less developed the gas emanations were stronger. Thicker
615 alluvial deposits were found to be less representative of the deep end-member due to more
616 pronounced interaction with these formations. Gas migration from depth is a highly complex
617 phenomenon that must be better constrained in order to build confidence in safety rules and
618 remediation strategies of CCS projects. Even at the upper level, near surface features have a
619 strong influence on degassing pattern as pointed out by coupled geochemical/geophysical
620 investigations (Schütze *et al.*, 2012).
621 Soil gas surveys performed under "point acquisition" schematic are relevant for the thorough
622 description of surface leakage over a restricted spatial array. They are not fully appropriate for
623 the monitoring of large areas and may be time consuming for repeated data acquisitions. They
624 do not allow to take into account for the variability linked to external causes such as climatic
625 variability and its imprint on surface environments. They are nonetheless crucial to best settle
626 monitoring equipment for long-term surveillance. Investigation done at Sainte-Marguerite
627 was mostly oriented on the ^{222}Rn specie. It allowed highlighting excursion from background
628 noise under "gas burst" event. Such events were characterised by influence radius of at least
629 200 m. Scaling effects in case of leakage from CCS storage may not allow to get such
630 amounts of gases percolating up to the surface.
631 Therefore, there is also a need to monitor integrative bodies such as aquifers. In nearly all
632 cases, CCS sites are more or less deep and overlying aquifers exist. Monitoring aquifers in the

633 case of natural leaking analogues is from one side little frustrating as the initial composition
634 of the waters is not known – water properties prior leakage from a CCS site are known a
635 priori – but on the other hand these waters represent an opportunity to study deep degassing
636 through the interaction with water and rocks – that will be the case for CCS sites. The
637 harmonic pulsation of Geyser Brissac is an extreme case relying on the accumulation of gas
638 until the degassing due to overpressure.
639 Point monitoring of waters is by definition subject to heterogeneity of spatial coverage, ways
640 to collect samples being restricted to available outlets or wells. Constraints on chemical
641 processes occurring at depth may be brought by specific characterisation of the dissolved
642 constituents and by related isotopic systematics. Particularly, the determination of mixing
643 processes and their influence is important, as leakage from CCS site may be evidenced
644 through the mixing of the water from the storage complex and overlying aquifers. Such
645 methodology is not restricted to dissolved constituents and can also be extended to associate
646 gases such as ^{4}He (Gilfillan *et al.*, 2011).
647 As for soil gases, monitoring at regular frequency of water bodies is complementary with
648 point methods. Time scale of recording depends on the kinetic of the processes. At Sainte-
649 Marguerite such monitoring was performed at high frequency in order to take into account
650 variations over short time scales, cyclicity of the geyser being around 22 minutes. Most
651 prominent variations were stated for pH, dissolved oxygen, redox potential and dissolved CO_2
652 content. From soil gas measurements it was also stated that geyser "breathing" influences the
653 soil gas evolution over short periods at a radius close to 20-30 m.
654
655 Several conclusions arise when moving from analogue scale to industrial scale. Basically
656 studies devoted to CCS projects separate into baseline data acquisitions, then monitoring
657 actions during the injection and final monitoring operations after well closure and

abandonment. Baseline studies are essential as they represent the only data that will allow definition of anomalies during injection and post-injection. Establishing baseline values is a site-specific procedure but often their definition is based on a restricted dataset of measurement over limited time in order to match scientific issues on one side and industrial approach on the other side.

Natural analogue monitoring suggests that data acquisition should not be restricted in narrow perimeters above the storage complex itself but should encompass all the areas that may potentially be affected by leakage. One of the main concerns is the capability of the monitoring system to detect potential leaks. Anomalies are often restricted on narrow areas at surface and deploying monitoring devices on such small grids (20 to 200 m of array) is absolutely unrealistic if only considering costs. At surface, apart from such a net, it is therefore hypothetical to ensure a safely monitoring over great distances simply using punctual and point methods. Installation of equipment just above a potential leaking pathway that may not have been recognized by geological studies would be too lucky to be reproduced regularly over several deep CO_2 storages. Surveying methodologies are nowadays adapted to integrate gas emanations characteristics from hectometer to kilometer scales. Methods such as eddy covariance, open path laser, airborne hyper-spectral monitoring etc… are promising ones but until now they are not as robust as required for storages monitoring as they are often dependent from modeling of the atmosphere compartment that is strongly turbulent over short time periods and may therefore induce undesirable effects and false warnings (*e.g.* Klusman, 2011).

Ways to overcome this limitation may be of several types. Monitoring at depth through boreholes, using geochemical and/or geophysical methods, appears to be the best way to get early detection and warning of unexpected events by focusing on the water phase and on dissolved gas contents. Monitoring should be performed under continuously deployed devices

683 or at least consisting in repeated measurements. Nevertheless, from a geochemical point of
684 view, lot of the available monitoring equipment that may be deployed at depth has nowadays
685 not reached the desirable level of reliability over long time periods.
686 Many efforts have been done in recent years to adapt technologies to CCS monitoring and to
687 gain confidence in results, but long-term recording of parameters remains a challenging
688 question.
689
690
691 **Acknowledgments**
692 This research was conducted through the fundings of French Research Agency projects
693 Geocarbone Monitoring (2006-2008) and Sentinelle (2008-2011). Anne Bonhomme (Les
694 Mousquetaires Group) is warmly thanked to allow the access to the Sainte-Marguerite site and
695 subsequently fruitful data acquisition. BRGM people that performed laboratory analyses are
696 gratefully acknowledged.
697 Two anonymous reviewers and the associate editor are also warmly thanked for their help in
698 improving the manuscript.
699
700 **References**
701 Al-Hilal M., Sbeinati M. R., Darawcheh R. (1998) Radon variations and microearthquakes in
702 Western Syria. Applied Radiation and Isotopes, 49, 117-123.
703
704 Appora-Gnekindy I. (1992) Etude spatiale et temporelle des émanations gazeuses de quelques
705 zones thermominérales du Massif Central Français, rapport de stage BRGM, 92 p.
706

Bachu S. (2003) Screening and ranking of sedimentary basins for sequestration of CO_2 in geologic media, Environmental Geology 44(3), 277-289.

Batard F., Billet C., Risler J.J. (1978) Prospection de CO_2 d'origine profonde dans le Massif Central, rapport BRGM 78-SGN-466-MCE, 16 p.

Battani A., Deville E., Faure J.-L., Noirez S., Tocqué E., Jeandel E., Benoît Y., Schmitz J., Parlouar D., Gal F., Le Pierrès K., Brach M., Braibant G., Bény C., Pokryszka Z., Charmoille A., Bentivegna G., Pironon J., de Donato P., Garnier C., Cailteau C., Barrès O., Radilla G., Bauer A. (2010) Geochemical study of the natural CO_2 emissions in the French Massif Central: How to predict origin, processes and evolution of CO_2 leakage, OGST, vol. 65, No 4, 615-633.

Baubron J.C., Mercier F., Rouzaire D. (1992) Eaux minérales de Sainte Marguerite (Puy de Dôme) – Prospection géochimique in situ des gaz des sols, Rapport BRGM R-36492-AUV-4S-92, 35 p.

Casanova J., Bodénan F., Négrel P., Azaroual M. (1999) Microbial control on the precipitation of modern ferrihydrite and carbonate deposits from the Cézallier hydrothermal springs (Massif Central, France), Sedimentary Geology 126, 125–145.

Chyi L. L., Chou C. Y., Yang F. T. et al. (2002) Automated radon monitoring of seismicity in a fault zone. Geofísica Internacional, 41, 507-511.

731 Das N. K., Bhandari R. K., Ghose D. et al. (2006) Explosive helium burst in thermal spring
732 emanations. Applied Radiation and Isotopes, 64, 144-148.
733
734 Dégranges P., Bosch B., Derec F. (1978) Hélium et sources thermominérales en France,
735 rapport BRGM 78-SGN-684-MCE, 22 p.
736
737 Fleischer R. L. (1981) Dislocation model for radon response to distant earthquakes.
738 Geophysical Research Letters, 8, 477-480.
739
740 Fleischer R. L., Mogro-Campero A. (1985) Association of subsurface radon changes in
741 Alaska and the northeastern United States with earthquakes. Geochimica et Cosmochimica
742 Acta, 49, 1061-1071.
743
744 Fouillac, C., Michard, G. (1981) Sodium/lithium ratio in water applied to geothermometry of
745 geothermal reservoirs. Geothermics 10, 55–70.
746
747 Fouillac C. (1983) Chemical geothermometry in CO_2-rich thermal waters. Example of the
748 French Massif Central, Geothermics, Vol. 12, No. 2/3, 149 – 160.
749
750 Fouillac C., Fouillac A.M., Chery L. (1991) lsotopic studies of deep and surface waters in the
751 French Massif Central, Proceedings of isotope techniques in water resources development,
752 Vienne, 11-15/03/1991, 646-648.
753
754 Gal F., Gadalia A. (2011) Mesure des gaz des sols autour du système volcanique le plus
755 récent de France métropolitaine (lac Pavin, Massif Central). Soil gas measurements around

the most recent volcanic system of metropolitan France (lake Pavin, Massif Central), C. R. Geosciences 343, 43-54.

Gal F., Brach M., Braibant G., Jouin F., Michel K. (2011) CO_2 escapes in the Laacher See region, East Eifel, Germany: application of natural analogue onshore and offshore geochemical monitoring, International Journal of Greenhouse Gas Control, 5, 1099-1118.

Gerlach T. M., Taylor B. E. (1990) Carbon isotope constraints on degassing of carbon dioxide from Kilauea Volcano, GCA, 54, 2051-2058.

Ghosh D., Deb A., Sengupta R. et al. (2007) Pronounced soil-radon anomaly - Precursor of recent earthquakes in India. Radiation Measurements, 42, 466-471.

Gilfillan S.M.V., Wilkinson M., Haszeldine R.S., Shipton Z.K., Nelson S.T., Poreda R.J. (2011) He and Ne as tracers of natural CO_2 migration up a fault from a deep reservoir, International Journal of Greenhouse Gas Control, 5, 1507-1516.

Jeandel E., Battani A., Sarda P. (2010) Lessons learned from natural and industrial analogues for storage of carbon dioxide, International Journal of Greenhouse Gas Control, 4, 890-899.

Kharatian K., Travi Y., Igoumnov V. (2002) Activité du gaz radon dans l'air du sol et sismicité locale : exemple du bassin de l'Arax (Arménie). Comptes Rendus de Geosciences, 334, 179-185.

780 Klusman R.W. (2011) Comparison of surface and near-surface geochemical methods for
781 detection of gas microseepage from carbon dioxide sequestration, International Journal of
782 Greenhouse Gas Control, 5, 1369-1392.
783
784 Krüger M., Jones D., Frerichs J., Oppermann B.I., West J., Coombs P., Green K., Barlow T.,
785 Lister R., Shaw R., Strutt M., Möller I. (2011) Effects of elevated CO_2 concentrations on the
786 vegetation and microbial populations at a terrestrial CO_2 vent at Laacher See, Germany,
787 International Journal of Greenhouse Gas Control 5, 1093-1098.
788 Lemieux J.-M. (2011) Review: The potential impact of underground geological storage of
789 carbon dioxide in deep saline aquifers on shallow groundwater resources, Hydrogeology
790 Journal, 19, 757-778.
791
792 Lewicki J.L., Birkholzer J., Tsang C.-F. (2007) Natural and industrial analogues for leakage
793 of CO_2 from storage reservoirs: identification of features, events, and processes and lessons
794 learned, Environ Geol, 52, 457-467.
795
796 Mercier F., avec la collaboration de Ausseur Y. (1987) Fichier des eaux minérales du Puy de
797 Dôme, rapport BRGM 87-SGN-780-AUV, 222 p.
798
799 Merle O., Michon L. (2001) The formation of the West European Rift: A new model as
800 exemplified by the Massif central area, Bull. Soc. Géol. France, 172, 2, 81-89.
801
802 Michard G., Evrard M., Fouillac C., Lambert B. (1978) Acquisition des ions alcalino-terreux
803 par les eaux carbogazeuses, Earth Planet. Sci. Lett. 41, 170–174.
804

Michard G. (1979) Géothermomètres chimiques. Bull. Du BRGM (2ème série) Section III 2, 183–189.

Michard G., Fouillac C., Grimaud D., Denis J. (1981) Une méthode globale d'estimation des températures des réservoirs alimentant les sources thermales. Exemple du Massif Central Français, Geochimica et Cosmochimica Acta, 45, 1199-1207.

Michard G. (1990) Behaviour of major elements and some trace elements (Li, Rb, Cs, Sr, Fe, Mn, W, F) in deep hot waters from granitic areas. Chem. Geol. 89, 117–134.

Michel-Le Pierrès K., Gal F., Brach M., Guignat S. (2010) Radon, Helium and CO_2 measurements in soils overlying a former exploited oilfield, Pechelbronn district, Bas-Rhin, France, J. Env. Rad. 101, 835-846.

Négrel P., Fouillac C., Brach M. (1997a) Occurrence of mineral water springs in the the Allier River (Massif Central, France): stream channel of chemical and Sr isotope constraints, Journal of Hydrology 203, 143-153.

Négrel P., Fouillac C., Brach M. (1997b) Variations spatio-temporelles de la composition chimique et des rapports $^{87}Sr/^{86}Sr$ des eaux minérales de la Limagne d'Allier, C. R. Acad. Sci. Paris, 325, 119-124.

Ramola R. C., Prasad Y., Prasad G. et al. (2008) Soil-gas radon as seismotectonic indicator in Garhwal Himalaya. Applied Radiation and Isotopes, 66, 1523-1530.

Riding J.B., Rochelle C.A. (2009) Subsurface characterisation and geological monitoring of the CO_2 injection operation at Weyburn, Saskatchewan, Canada, Geological Society, London, Special Publications, 313, 227-256.

Rihs S., Condomines M., Poidevin J.L. (2000) Long-term behaviour of continental hydrothermal systems: U-series study of hydrothermal carbonates from the French Massif Central (Allier Valley), Geochimica et Cosmochimica Acta, Vol. 64, No. 18, 3189–3199.

Schütze C., Sauer U., Beyer K., Lamert H., Bräuer K., Strauch G., Flechsig Ch., Kämpf H., Dietrich P. (2012) Natural analogues: a potential approach for developing reliable monitoring methods to understand subsurface CO_2 migration processes, Environ. Earth Sci., DOI 10.1007/s12665-012-1701-4.

Spangler L.H. (2010) Foreword to the Special Issue on Zero Emission Research and Technology Center testing field site, Bozeman, Montana, USA, Environ. Earth Sci. 60, 225.

Stettler A. (1977) ^{87}Rb-^{87}Sr systematic of a geothermal water-rock association in the Massif Central, France. Earth and Planet. Sci, Lett., 34, 432-438.

Truesdell A.H. (1975) Geochemical techniques in exploration, summary of section III, In: Proceedings Second United Nation Symposium on the development and use of geothermal resources, vol. 1, pp. Iiii–Ixiii.

Wattananikorn K., Kanaree M., Wiboolsake S. (1998) Soil gas radon as an earthquake precursor: some considerations on data improvement. Radiation Measurements, 29, 593-598.

Figure captions:

Figure 1: location of the study area: dots locate points where soil gas data are available: black dots refer to 2006-2010 data acquisitions, red contoured dots are from the 90's dataset. Red dots represent the main mineral waters that are labelled in the inset. Yellow dots (labelled 1 to 4) represent points where continuous monitoring was performed. Grey lines represent main roads.

Figure 2: O_2 – CO_2 relationship for the 2006-2010 soil gas measurements; the equimolar replacement line (1 mole CO_2 ⇔1 mole O_2) is represented. Model line corresponds to the regression line between the 2 species; the 95% confidence interval of the regression is also indicated.

Figure 3: relationships between Ar, N_2, O_2 and CO_2 concentrations (% vol.) on samples analysed using laboratory gas chromatography (samples from year 2007).

Figure 4: A: Relationships between CO_2, ^{222}Rn and ^{4}He in soil gas (2006-2010 dataset); B: detail of the CO_2 - ^{222}Rn relationship for low ^{222}Rn concentrations (lesser than 300,000 $Bq.m^{-3}$).

Figure 5: Relationships between CO_2, ^{222}Rn and ^{4}He in soil gas.

Figure 6: spatial distribution of soil gas species (from left to right: CO_2, ^{222}Rn and ^{4}He) along with time (from top to bottom). Interpolation is done using natural neighbour contouring.

Figure 7: CO_2, ^{222}Rn and ^{4}He concentrations (2006 to 2010 measurements) recalculated in the 0 – 1 interval to lower the influence of ^{222}Rn and strengthen the one of ^{4}He (arbitrary units). See text for explanation.

Figure 8: a: temporal evolution of pressure for Barasol probes (labelled as F10X) for points 2 and 4 (Figure 1) and comparison with atmospheric data (Clermont-Ferrand Aulnat airport; http://french.wunderground.com/); b: evolution of soil temperatures and atmospheric temperature (same chart as for 8a); c: ^{222}Rn concentrations over time; blanked areas (F109 probe) correspond to power supply deficiency or to electronical malfunctioning of the ^{222}Rn detector.

Figure 9: F109 Barasol probe (point 4 in Figure 1); period from the 26 February 2009 to the 07 April 2009; a: temporal evolution of soil temperature and ^{222}Rn concentrations; b: temporal evolution of atmospheric pressure and ^{222}Rn concentrations; c: temporal evolution of atmospheric temperature and ^{222}Rn concentrations; d: spectral densities of ^{222}Rn concentrations; e and f: Principal Component Analysis using these 4 parameters.

Figure 10: a: temporal evolution of water temperature of Geyser Brissac during deployment; b: temporal evolution of temperature (°C), pH, specific conductance at 25°C ($mS.cm^{-1}$), dissolved oxygen content ($mg.L^{-1}$), redox potential (Eh, mV) and dissolved CO_2 (expressed as a mV value) during the second day of deployment.

903 **List of tables:**

904

905 Table 1: statistical parameters for the CO_2, ^{222}Rn and ^{4}He concentrations during the 90's and
906 2000's surveys (Sainte-Marguerite area; see Figure 1 for location).

907

908 Table 2: physico-chemical parameters of mineral waters from the Sainte-Marguerite area (see
909 location in Figure 1). Major ion contents are reported; blanks indicate a non-detection of the
910 specie or a non-measurement (isotope ratios). $\delta^{18}O$ and δD isotope ratios are reported as well
911 as the δD difference to the local meteoric water line ($\delta D = 8\ \delta^{18}O + 13.1$; Fouillac *et al.*,
912 1991). Equilibrium partial CO_2 pressure is computed using Diagrammes software
913 (http://www.lha.univ-avignon.fr/).

914

915 Table 3: descriptive statistics for ^{222}Rn concentrations acquired using Barasol probes.

916

917 Table 4: top: evolution of temperature (°C), pH, specific conductance at 25°C (EC, $mS.cm^{-1}$),
918 dissolved oxygen content ($mg.L^{-1}$), redox potential (Eh, mV) and dissolved CO_2 (expressed as
919 a mV value) along the 4 days of monitoring of the Geyser Brissac (monitoring duration
920 indicated into brackets); bottom: correlation matrix for each daily dataset. Geyser Brissac was
921 sampled on day 3 (Table 2).

N

Saladis springs

Allier River

1

2

3

4

old plant sp.

Tennis sp.

Valois sp.

Brissac Geyser

boreholes under exploitation

0 50 100

Metres

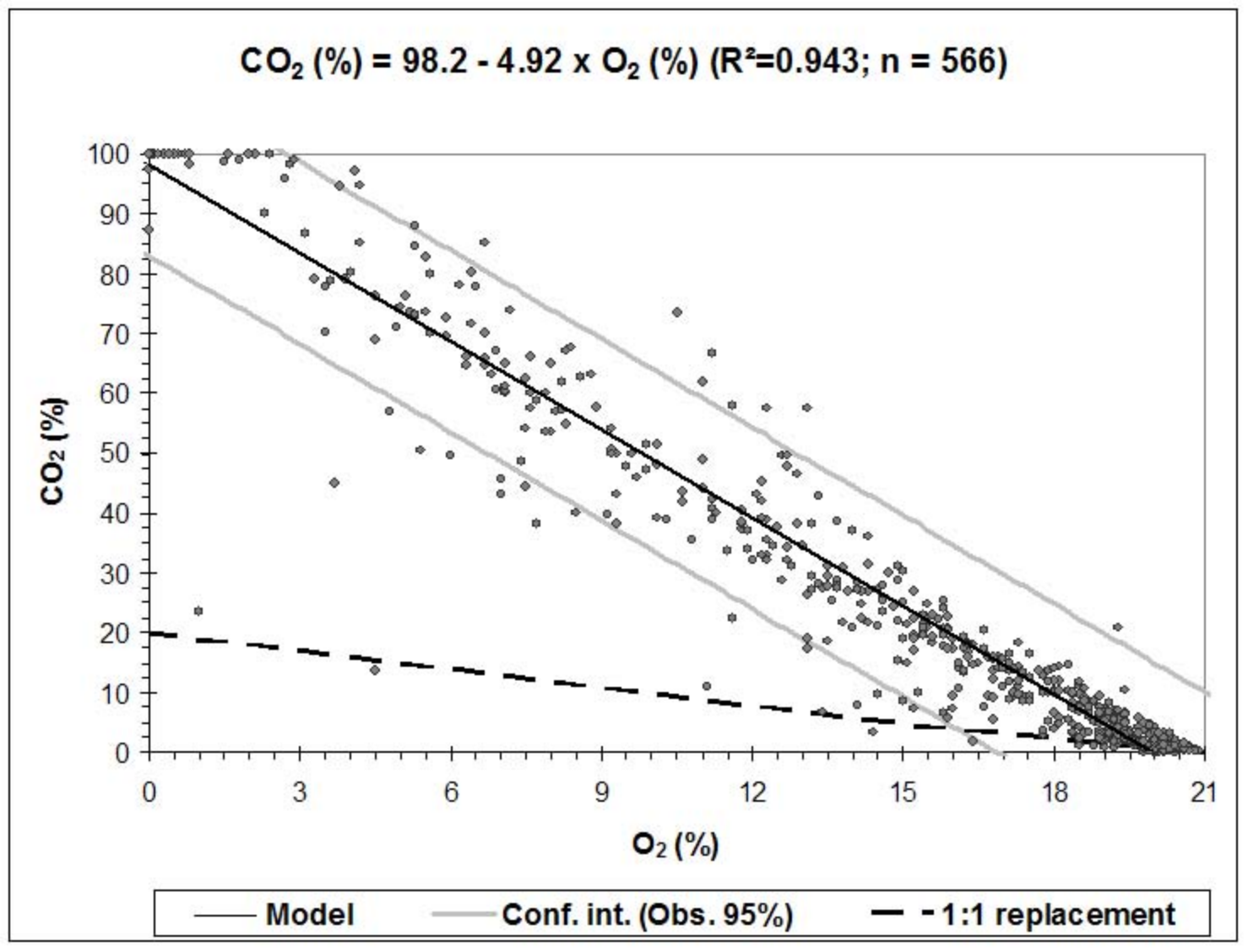
CO_2 (%) = 98.2 - 4.92 x O_2 (%) (R^2=0.943; n = 566)
100
90
80
70
60
50
40
30
20
10
0
CO_2 (%)
0
3
6
9
12
15
18
21
O_2 (%)
Model
Conf. int. (Obs. 95%)
1:1 replacement

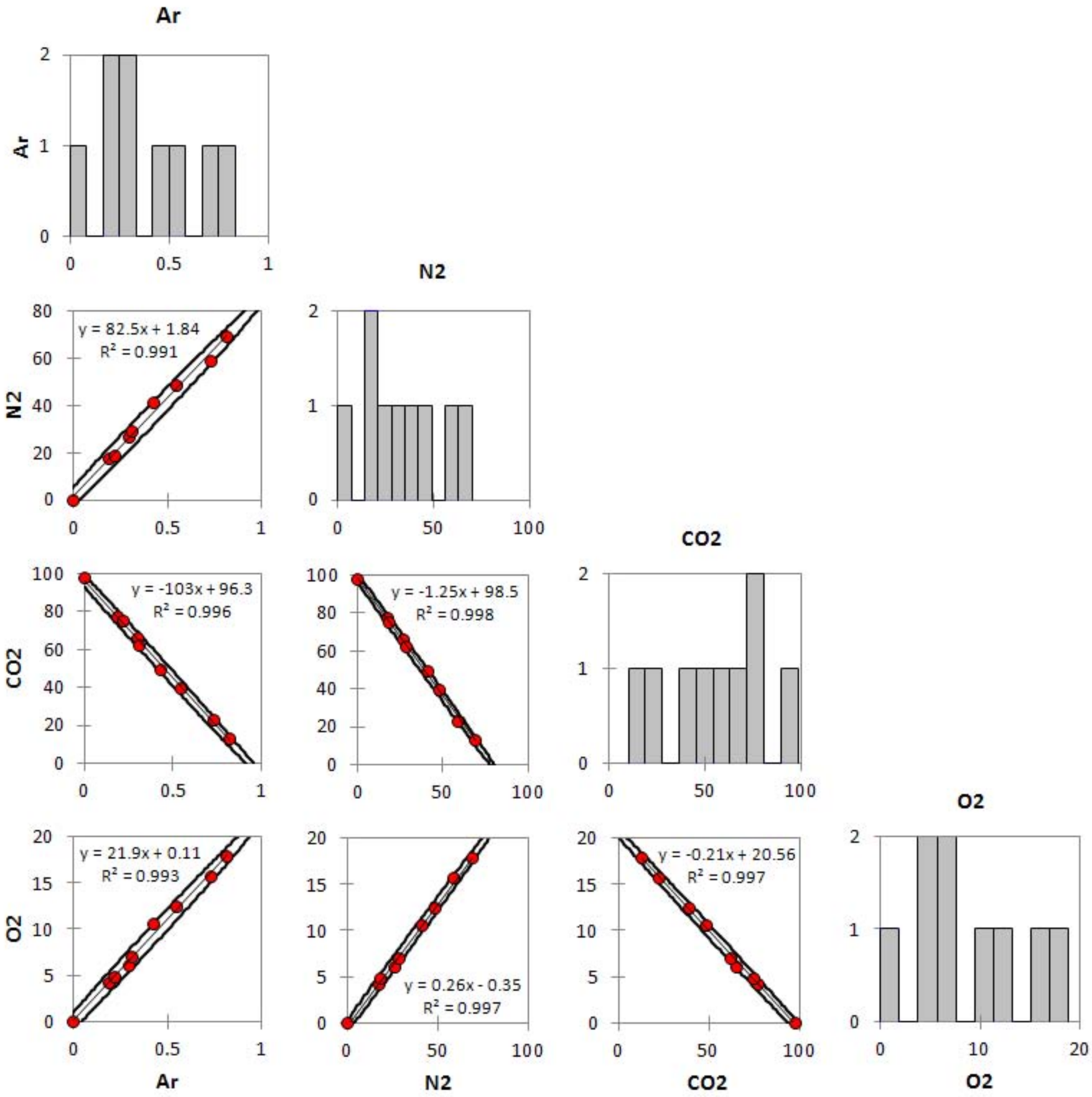
Ar
Ar
N2
y = 82.5x + 1.84
R² = 0.991
N2
CO2
y = -103x + 96.3
R² = 0.996
y = -1.25x + 98.5
R² = 0.998
CO2
O2
y = 21.9x + 0.11
R² = 0.993
y = 0.26x - 0.35
R² = 0.997
y = -0.21x + 20.56
R² = 0.997
O2
Ar
N2
CO2
O2

A)

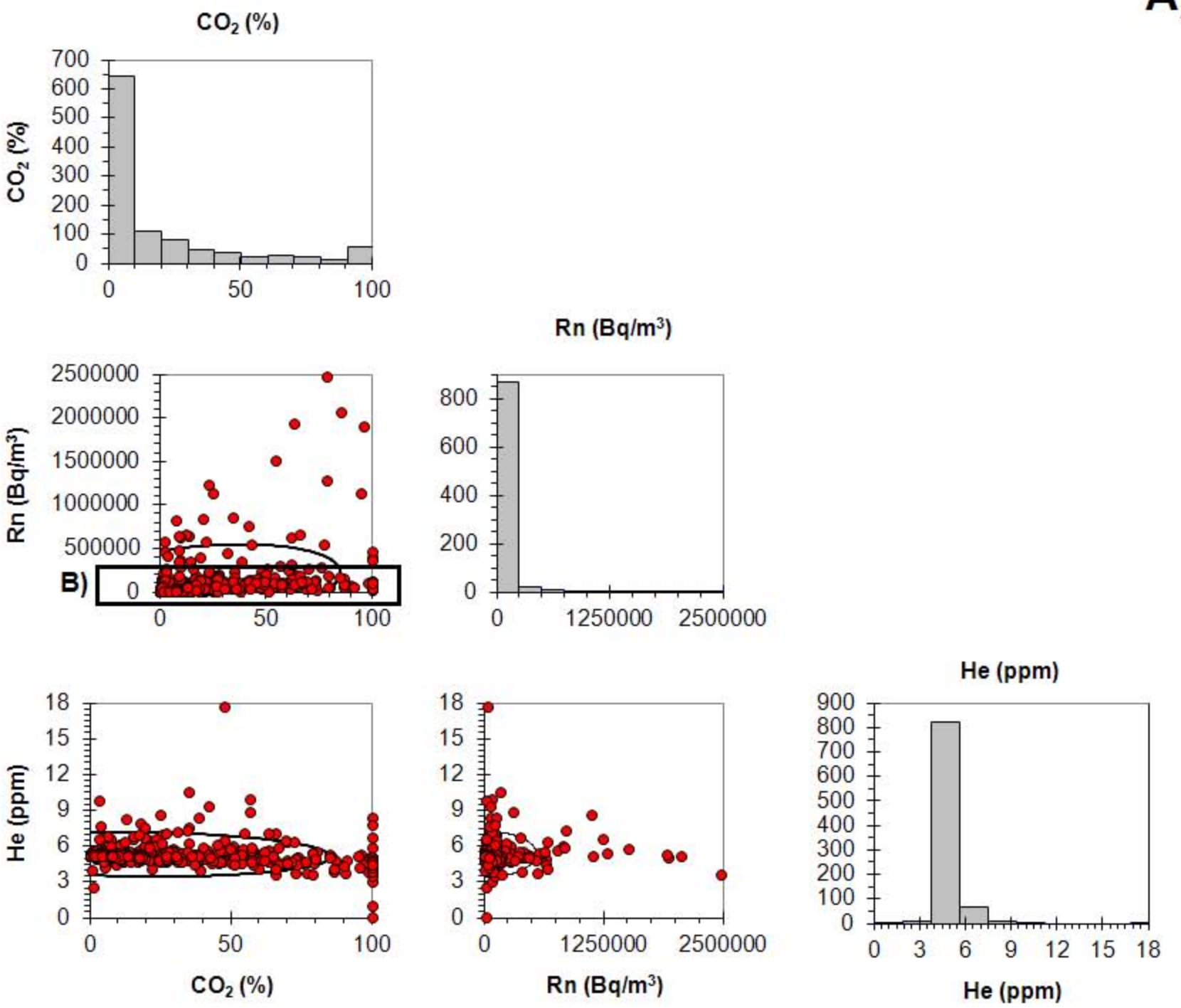
CO2 (%)
CO2 (%)
Rn (Bq/m3)
Rn (Bq/m3)
B)
He (ppm)
He (ppm)
CO2 (%)
Rn (Bq/m3)

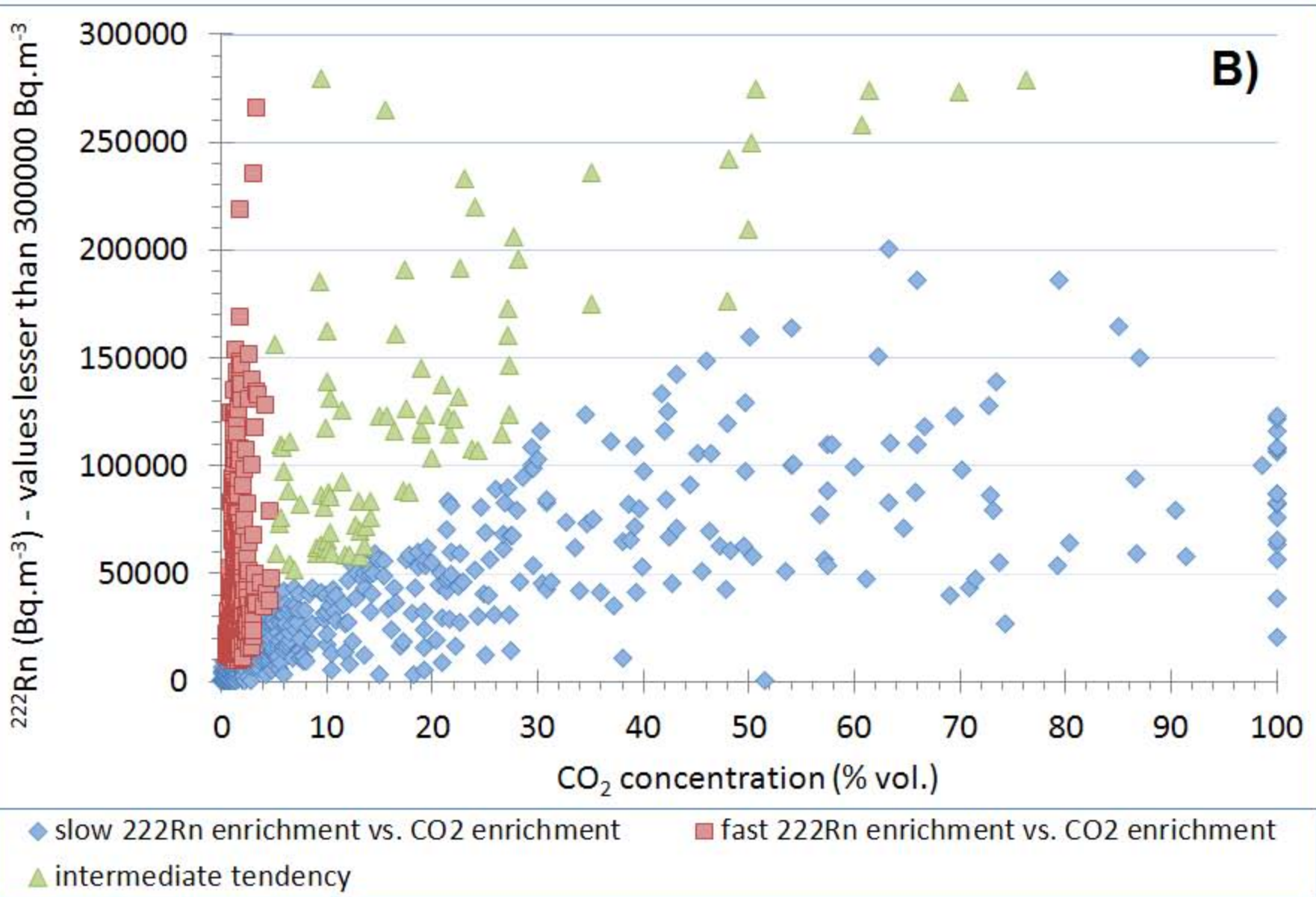
B)
222Rn (Bq.m-3) - values lesser than 300000 Bq.m-3
CO2 concentration (% vol.)
slow 222Rn enrichment vs. CO2 enrichment
fast 222Rn enrichment vs. CO2 enrichment
intermediate tendency

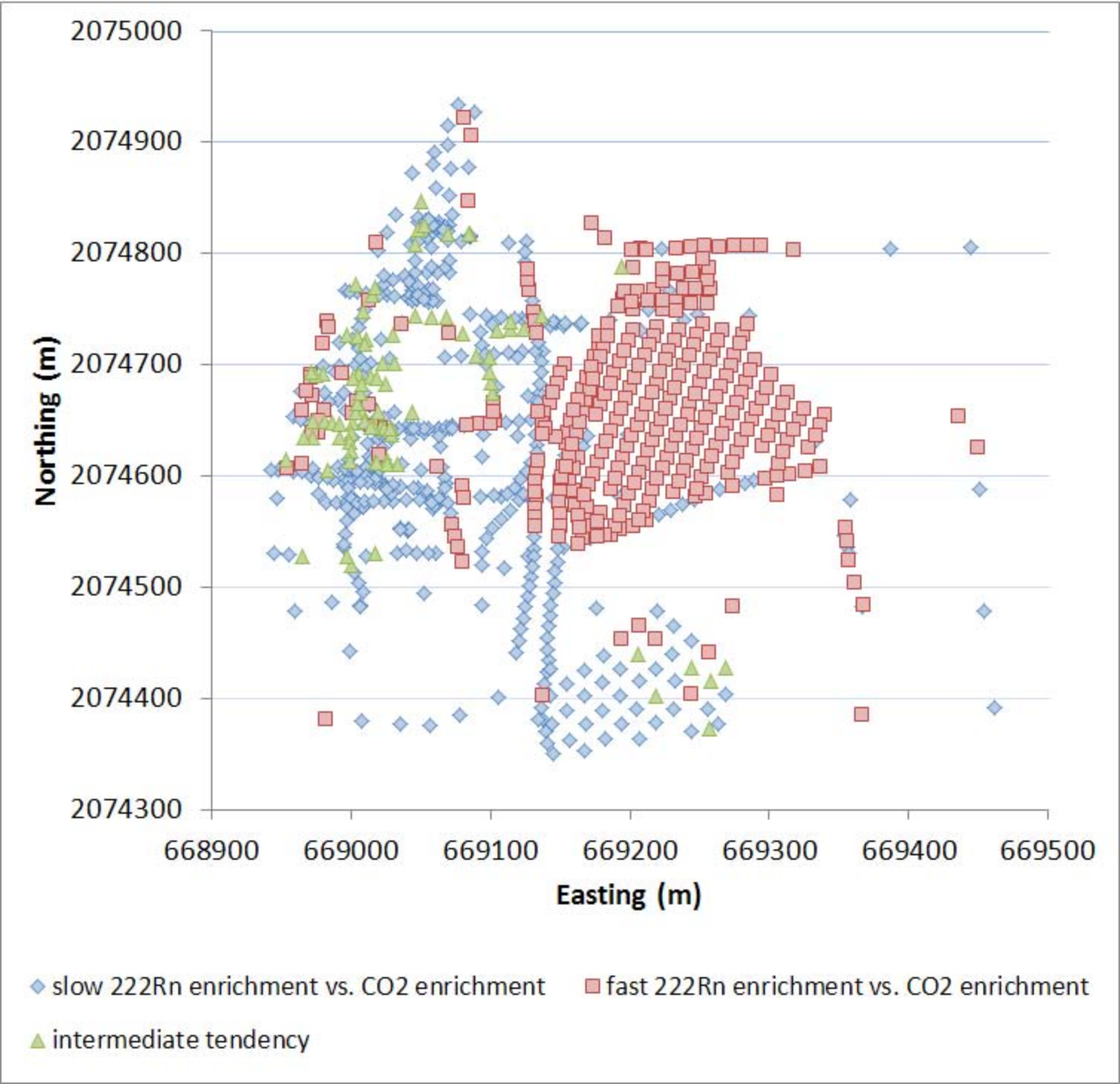
2075000
2074900
2074800
2074700
2074600
2074500
2074400
2074300
Northing (m)
668900
669000
669100
669200
669300
669400
669500
Easting (m)
slow 222Rn enrichment vs. CO2 enrichment
fast 222Rn enrichment vs. CO2 enrichment
intermediate tendency

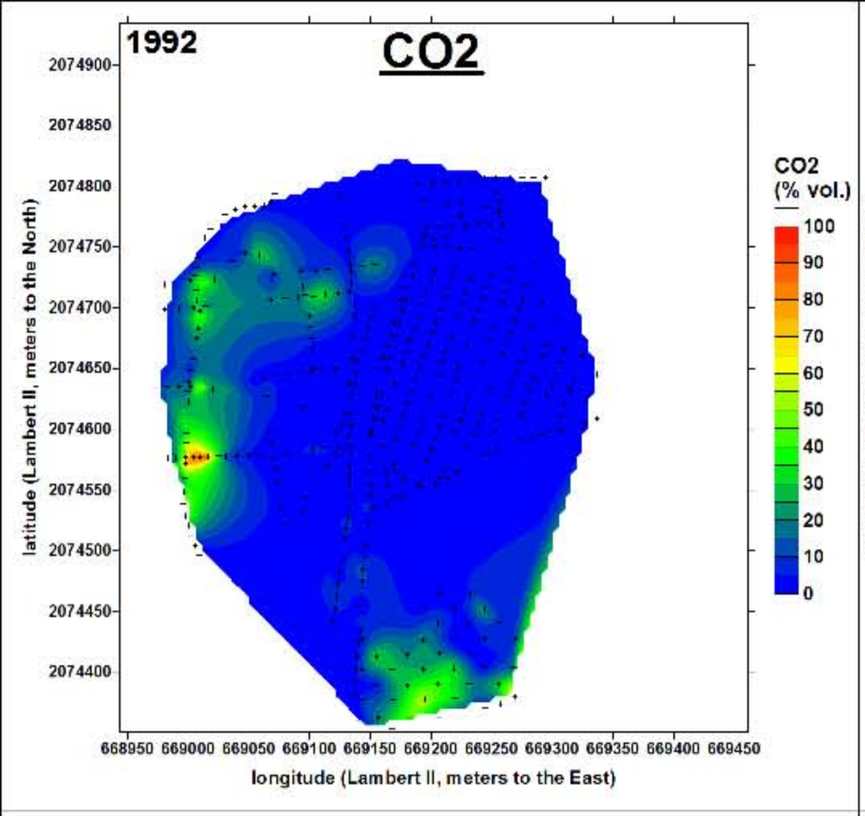
1992
CO2
latitude (Lambert II, meters to the North)
longitude (Lambert II, meters to the East)
CO2 (% vol.)
100
90
80
70
60
50
40
30
20
10
0

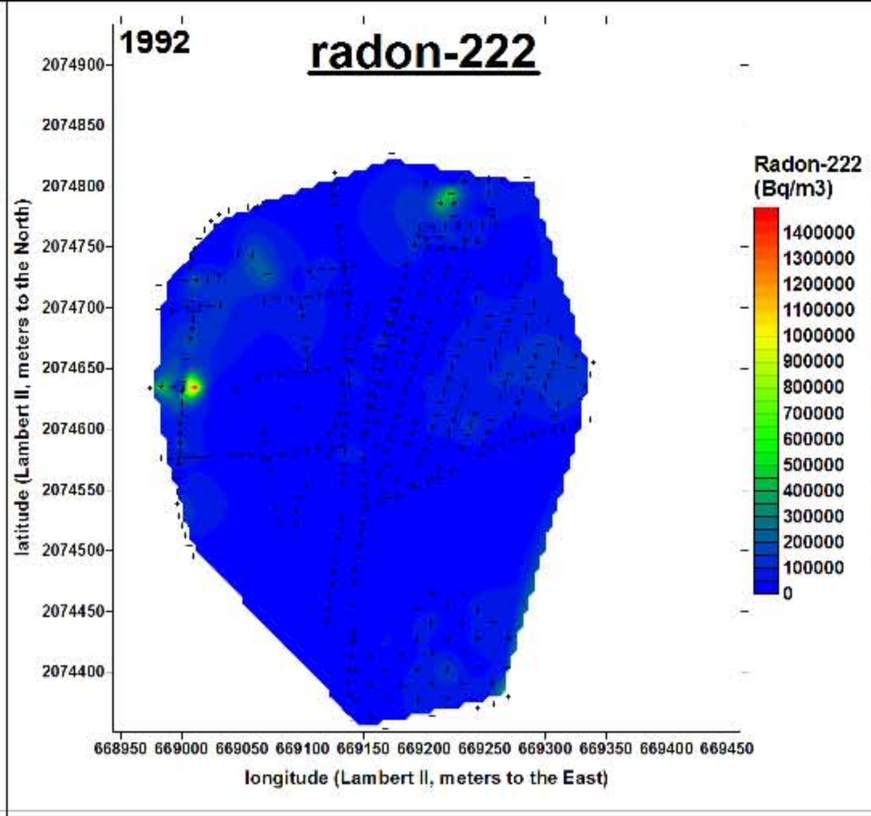
1992
radon-222
latitude (Lambert II, meters to the North)
longitude (Lambert II, meters to the East)
Radon-222 (Bq/m3)
1400000
1300000
1200000
1100000
1000000
900000
800000
700000
600000
500000
400000
300000
200000
100000
0

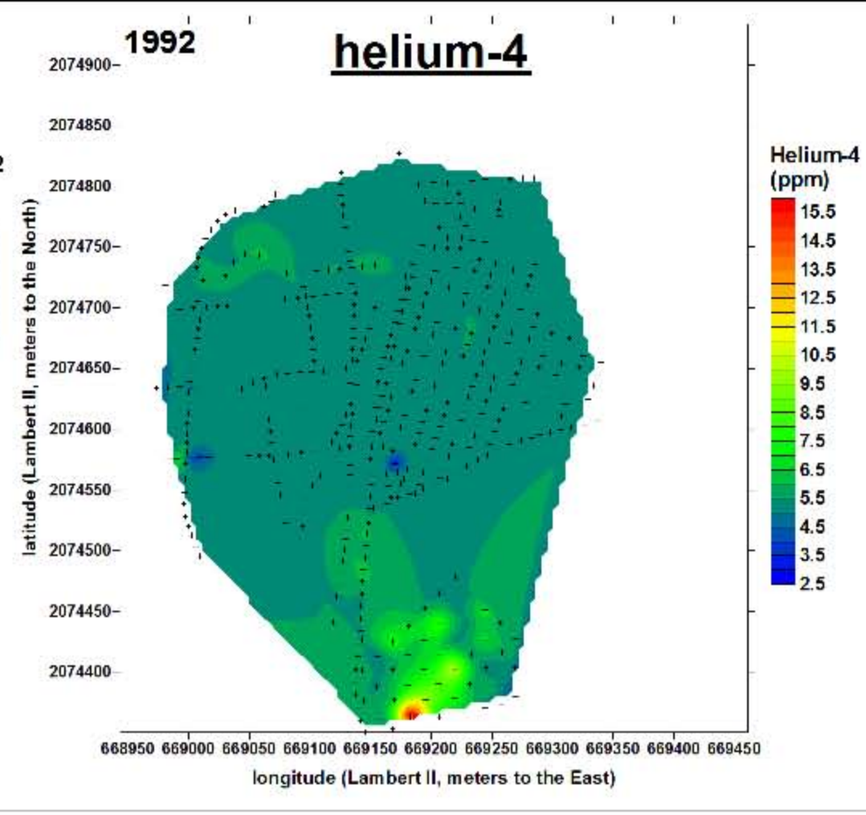
1992
helium-4
latitude (Lambert II, meters to the North)
longitude (Lambert II, meters to the East)
Helium-4 (ppm)
15.5
14.5
13.5
12.5
11.5
10.5
9.5
8.5
7.5
6.5
5.5
4.5
3.5
2.5

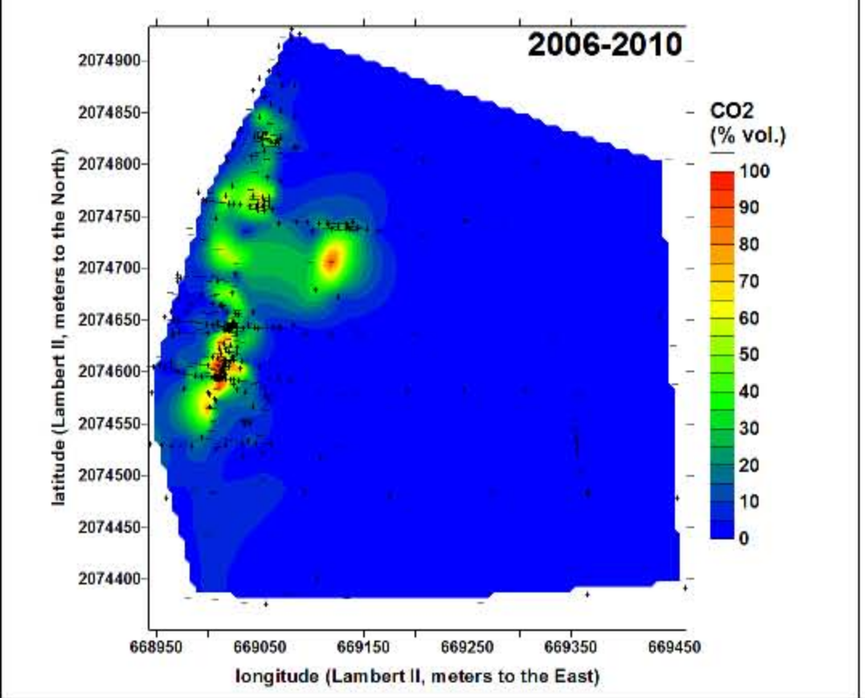
2006-2010
latitude (Lambert II, meters to the North)
longitude (Lambert II, meters to the East)
CO2 (% vol.)
100
90
80
70
60
50
40
30
20
10
0

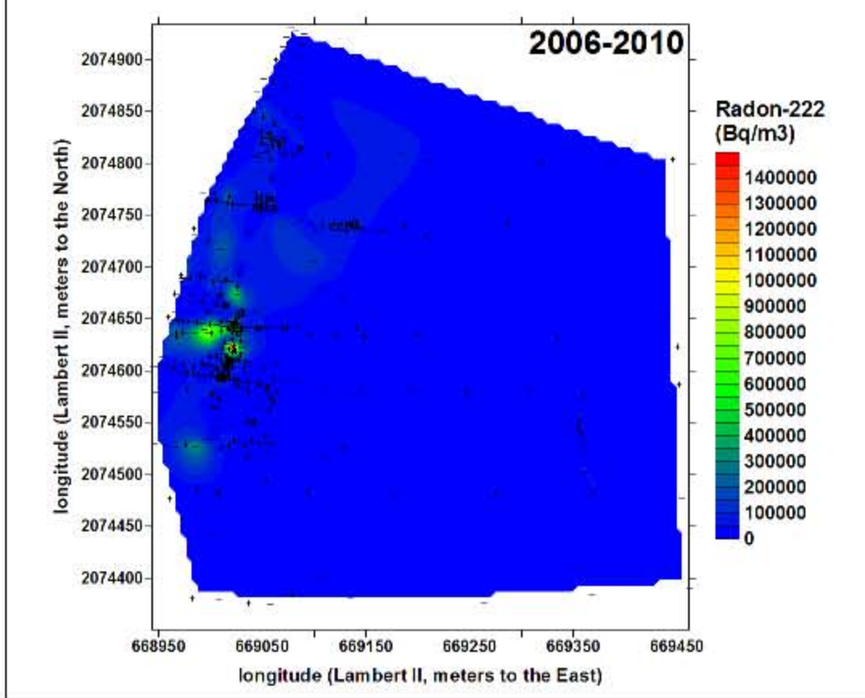
2006-2010
latitude (Lambert II, meters to the North)
longitude (Lambert II, meters to the East)
Radon-222 (Bq/m3)
1400000
1300000
1200000
1100000
1000000
900000
800000
700000
600000
500000
400000
300000
200000
100000
0

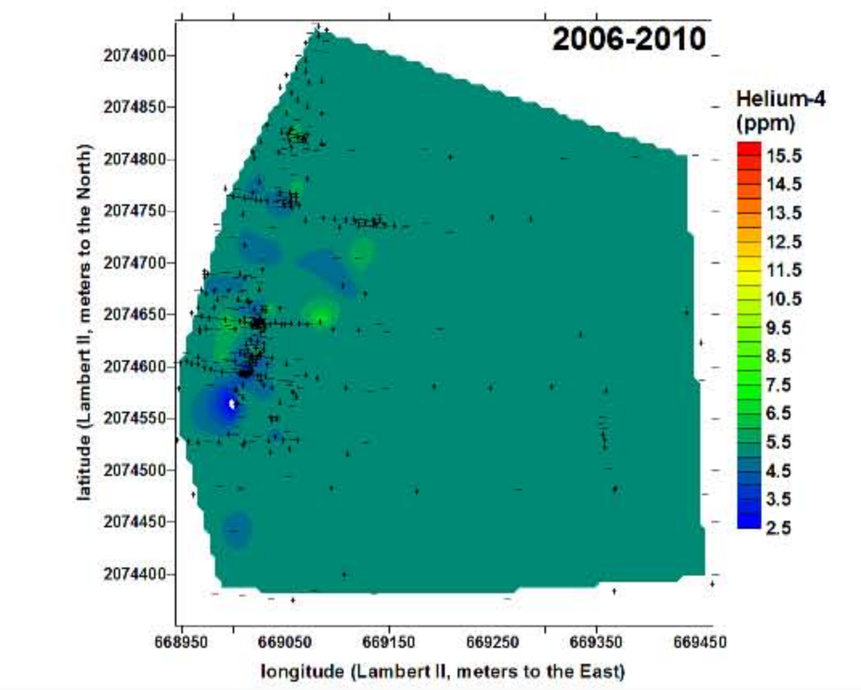
2006-2010
latitude (Lambert II, meters to the North)
longitude (Lambert II, meters to the East)
Helium-4 (ppm)
15.5
14.5
13.5
12.5
11.5
10.5
9.5
8.5
7.5
6.5
5.5
4.5
3.5
2.5

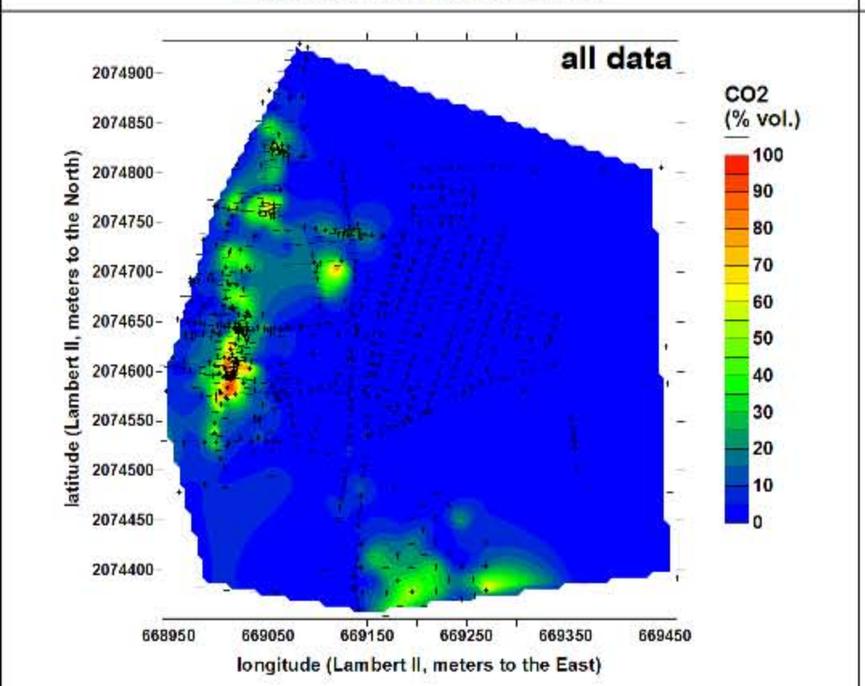
all data
latitude (Lambert II, meters to the North)
longitude (Lambert II, meters to the East)
CO2 (% vol.)
100
90
80
70
60
50
40
30
20
10
0

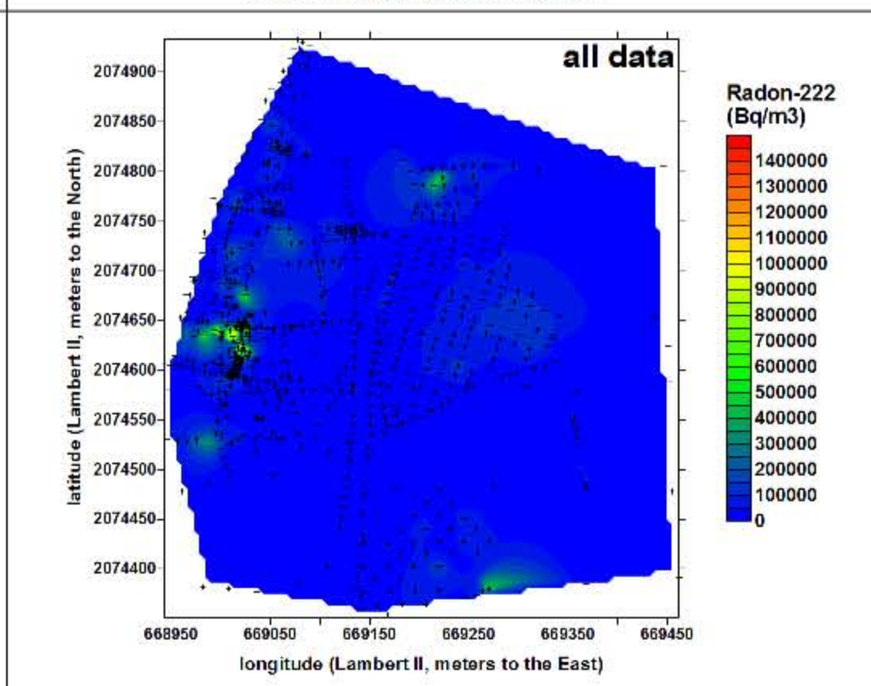
all data
latitude (Lambert II, meters to the North)
longitude (Lambert II, meters to the East)
Radon-222 (Bq/m3)
1400000
1300000
1200000
1100000
1000000
900000
800000
700000
600000
500000
400000
300000
200000
100000
0

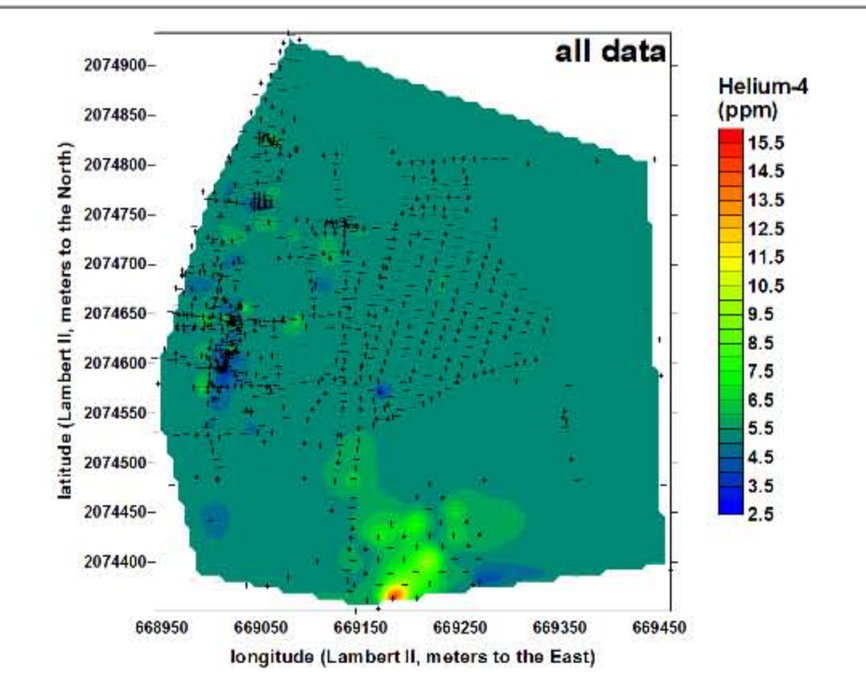
all data
latitude (Lambert II, meters to the North)
longitude (Lambert II, meters to the East)
Helium-4 (ppm)
15.5
14.5
13.5
12.5
11.5
10.5
9.5
8.5
7.5
6.5
5.5
4.5
3.5
2.5

colorscale: sum of CO2 + radon + helium fitted in the 0 - 1 interval
greyscale: CO2 distribution in the same interval

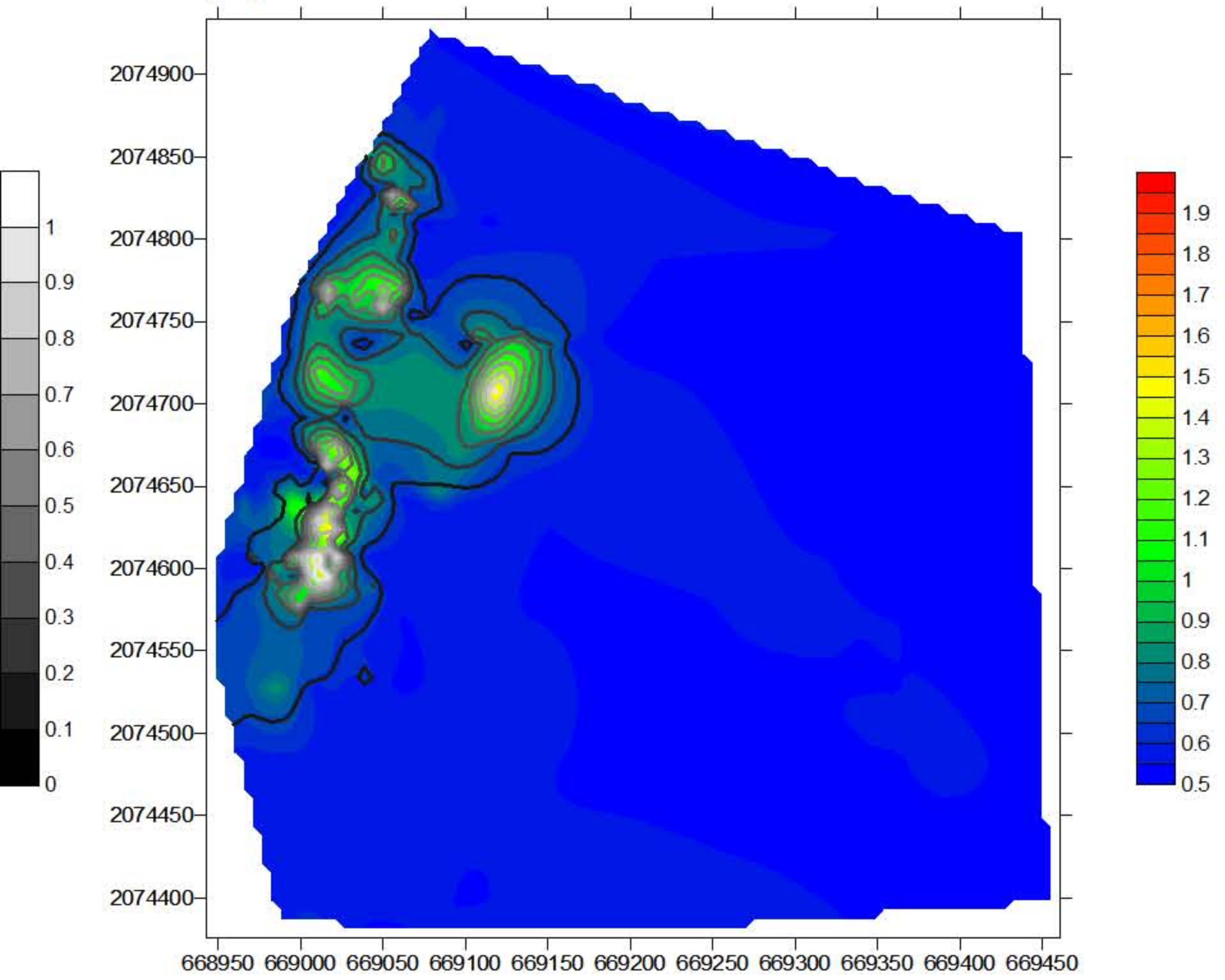

colorscale: sum of CO2 + radon + helium fitted in the 0 - 1 interval
greyscale: radon distribution in the same interval

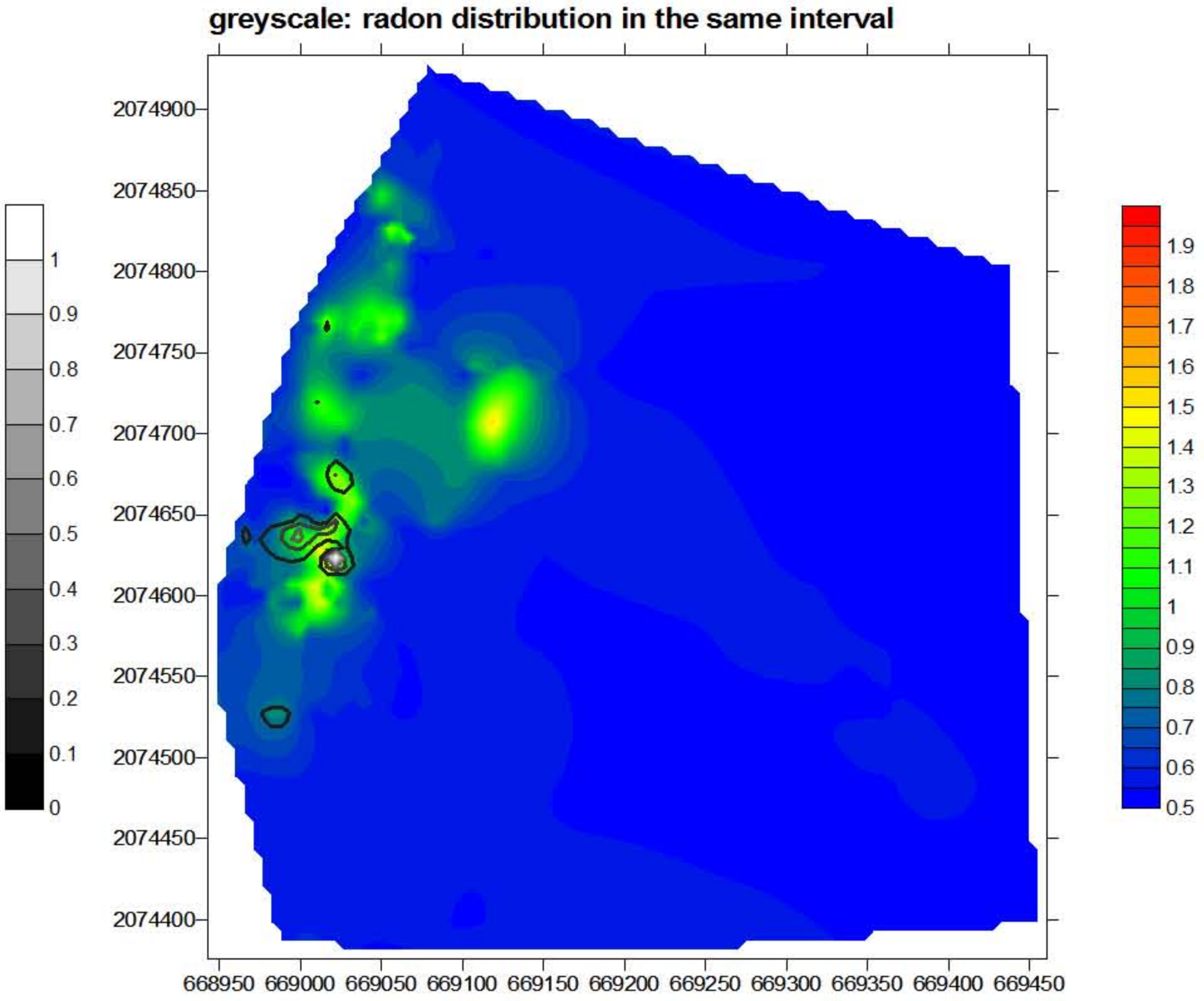

colorscale: sum of CO2 + radon + helium fitted in the 0 - 1 interval
greyscale: helium distribution in the same interval

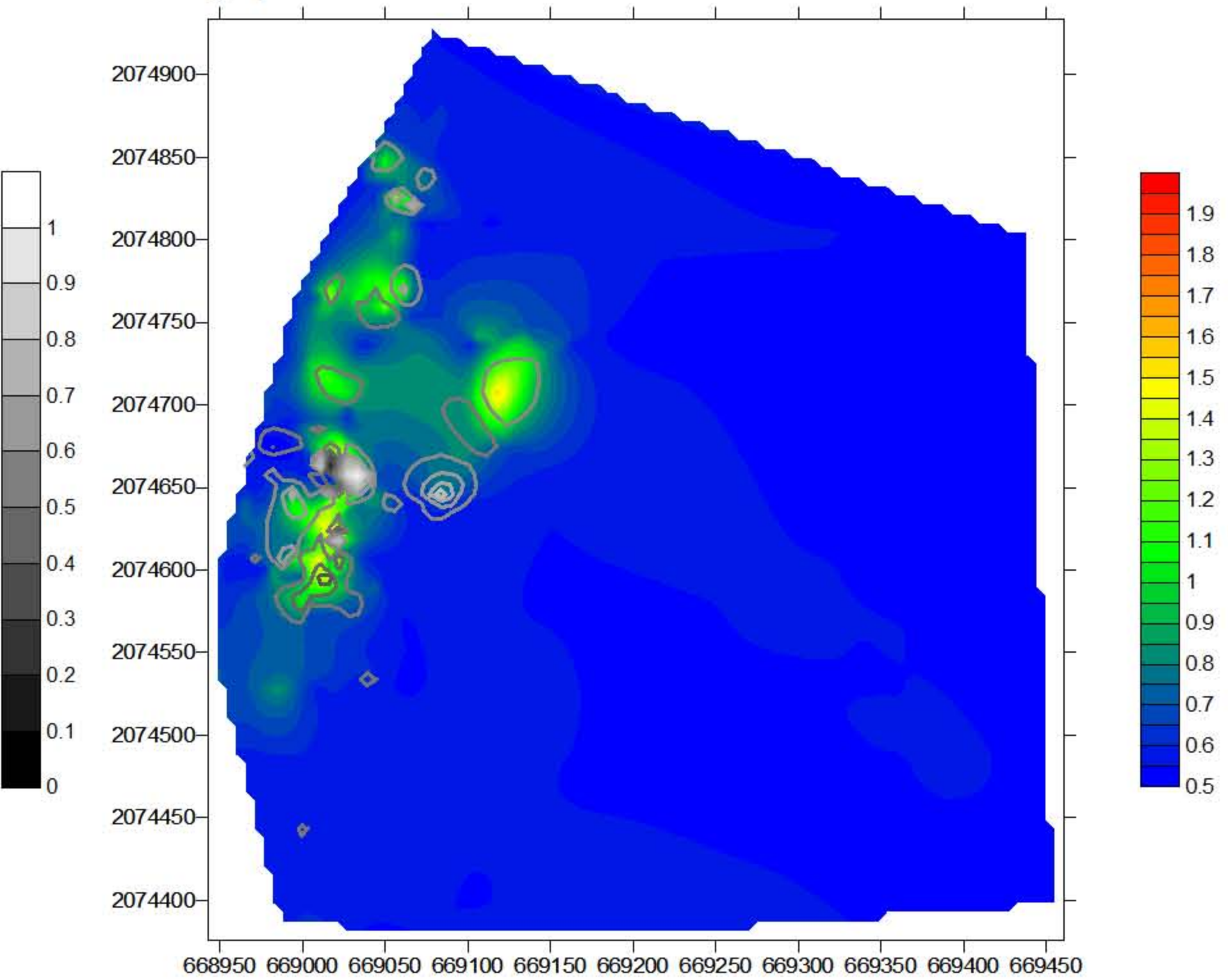

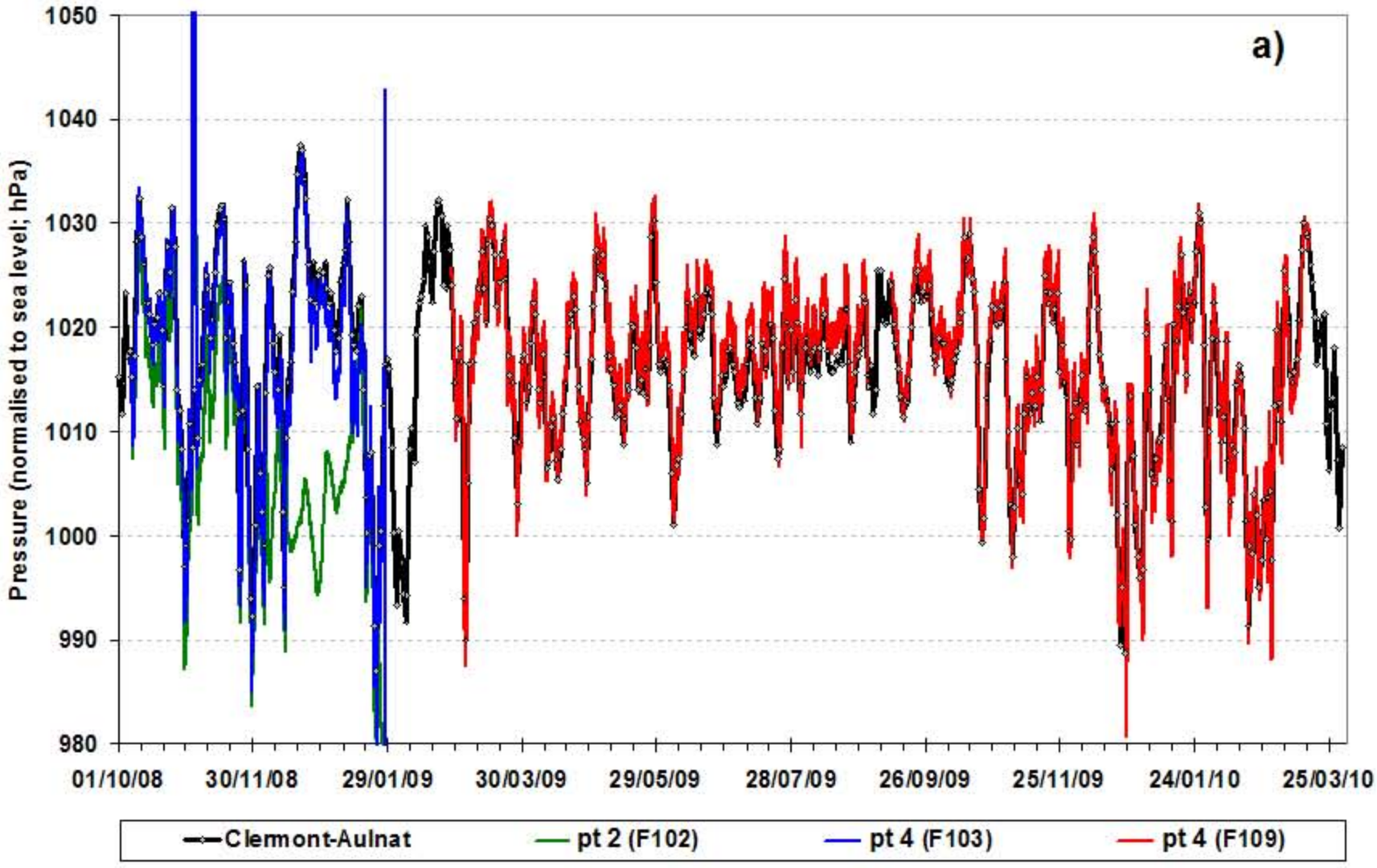
a)
Pressure (normalised to sea level; hPa)
1050
1040
1030
1020
1010
1000
990
980
01/10/08
30/11/08
29/01/09
30/03/09
29/05/09
28/07/09
26/09/09
25/11/09
24/01/10
25/03/10
Clermont-Aulnat
pt 2 (F102)
pt 4 (F103)
pt 4 (F109)

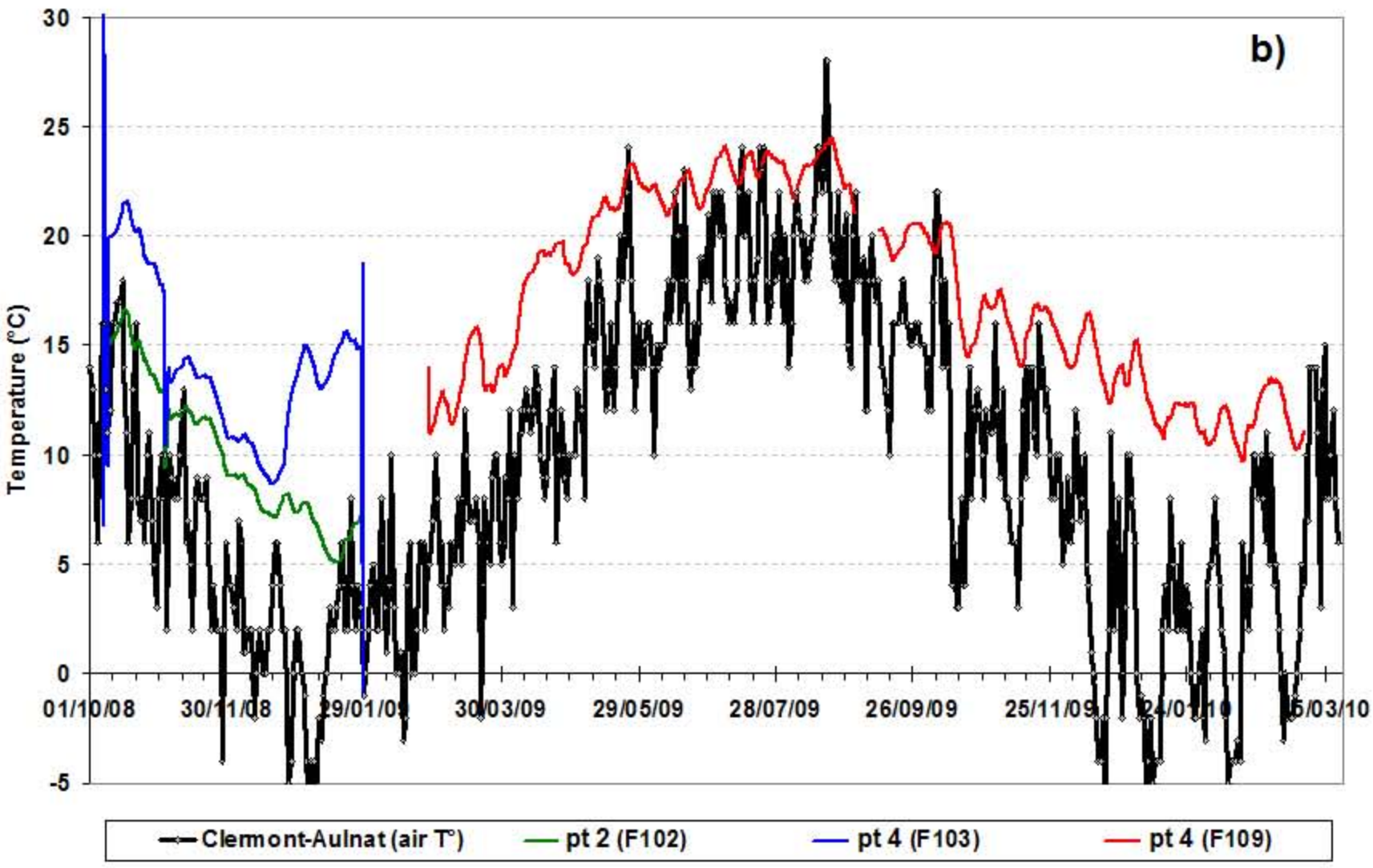
b)
Temperature (°C)
30
25
20
15
10
5
0
-5
01/10/08
30/11/08
29/01/09
30/03/09
29/05/09
28/07/09
26/09/09
25/11/09
24/01/10
25/03/10
Clermont-Aulnat (air T°)
pt 2 (F102)
pt 4 (F103)
pt 4 (F109)

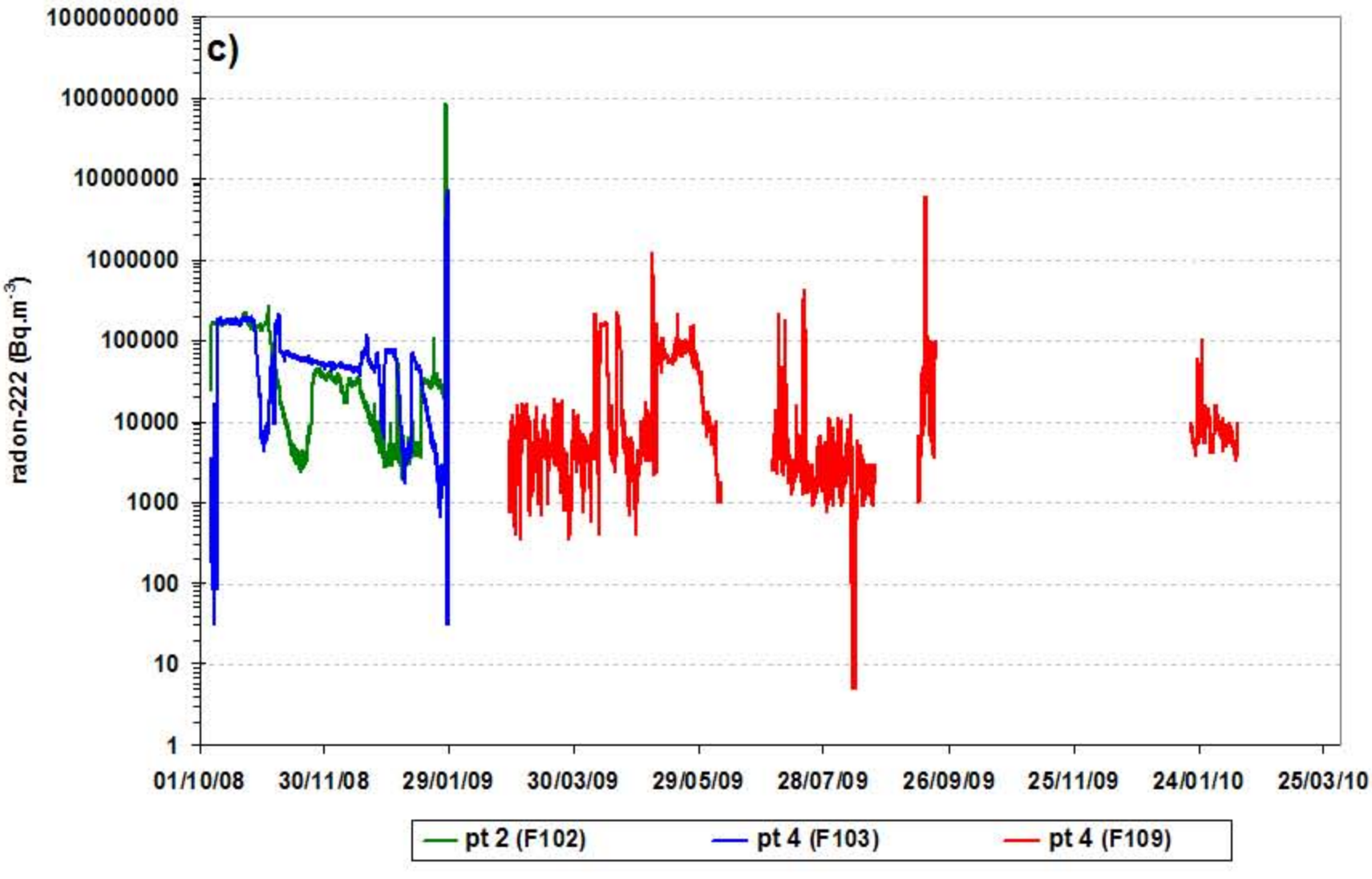
c)
radon-222 (Bq.m-3)
1000000000
100000000
10000000
1000000
100000
10000
1000
100
10
1
01/10/08
30/11/08
29/01/09
30/03/09
29/05/09
28/07/09
26/09/09
25/11/09
24/01/10
25/03/10
pt 2 (F102)
pt 4 (F103)
pt 4 (F109)

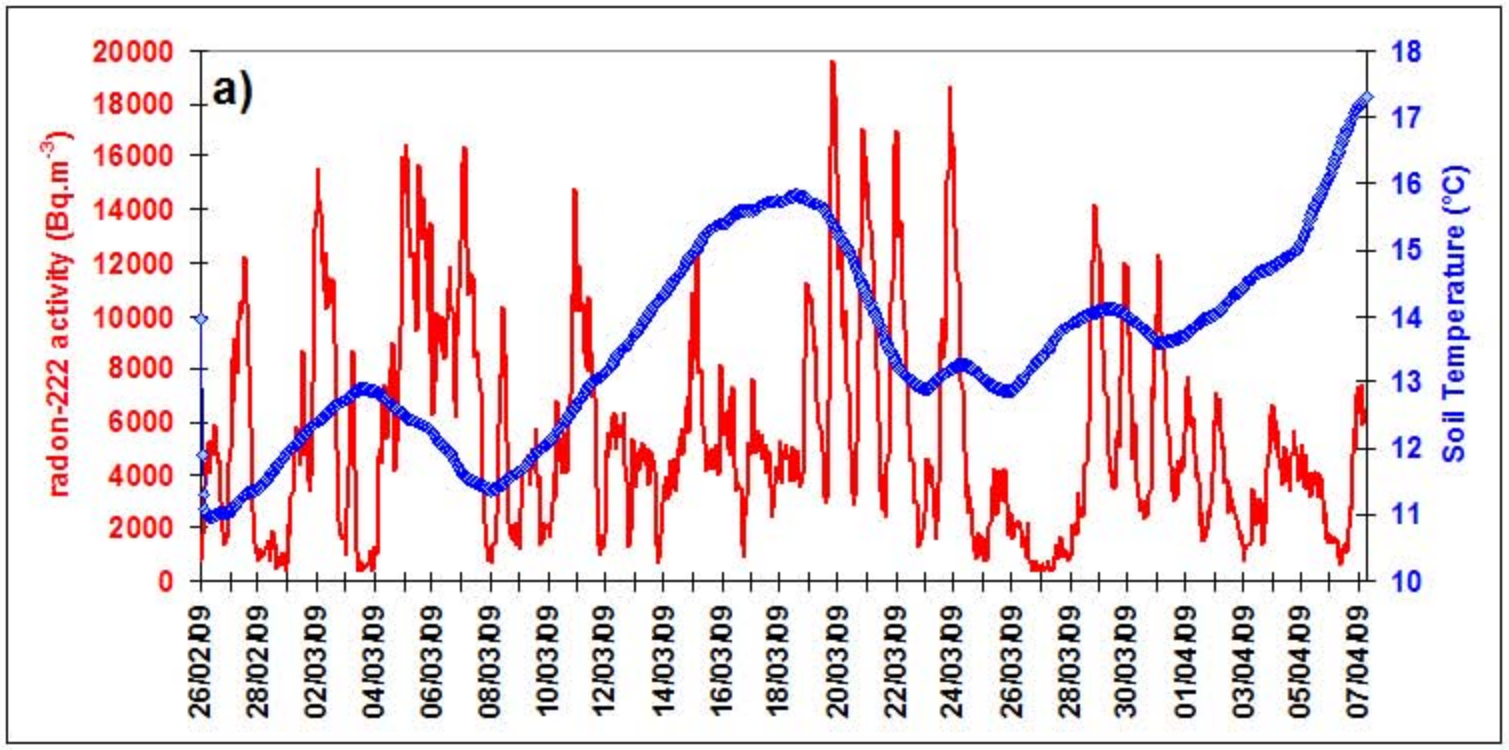
a)
radon-222 activity (Bq.m-3)
Soil Temperature (°C)
20000
18000
16000
14000
12000
10000
8000
6000
4000
2000
0
18
17
16
15
14
13
12
11
10
26/02/09
28/02/09
02/03/09
04/03/09
06/03/09
08/03/09
10/03/09
12/03/09
14/03/09
16/03/09
18/03/09
20/03/09
22/03/09
24/03/09
26/03/09
28/03/09
30/03/09
01/04/09
03/04/09
05/04/09
07/04/09

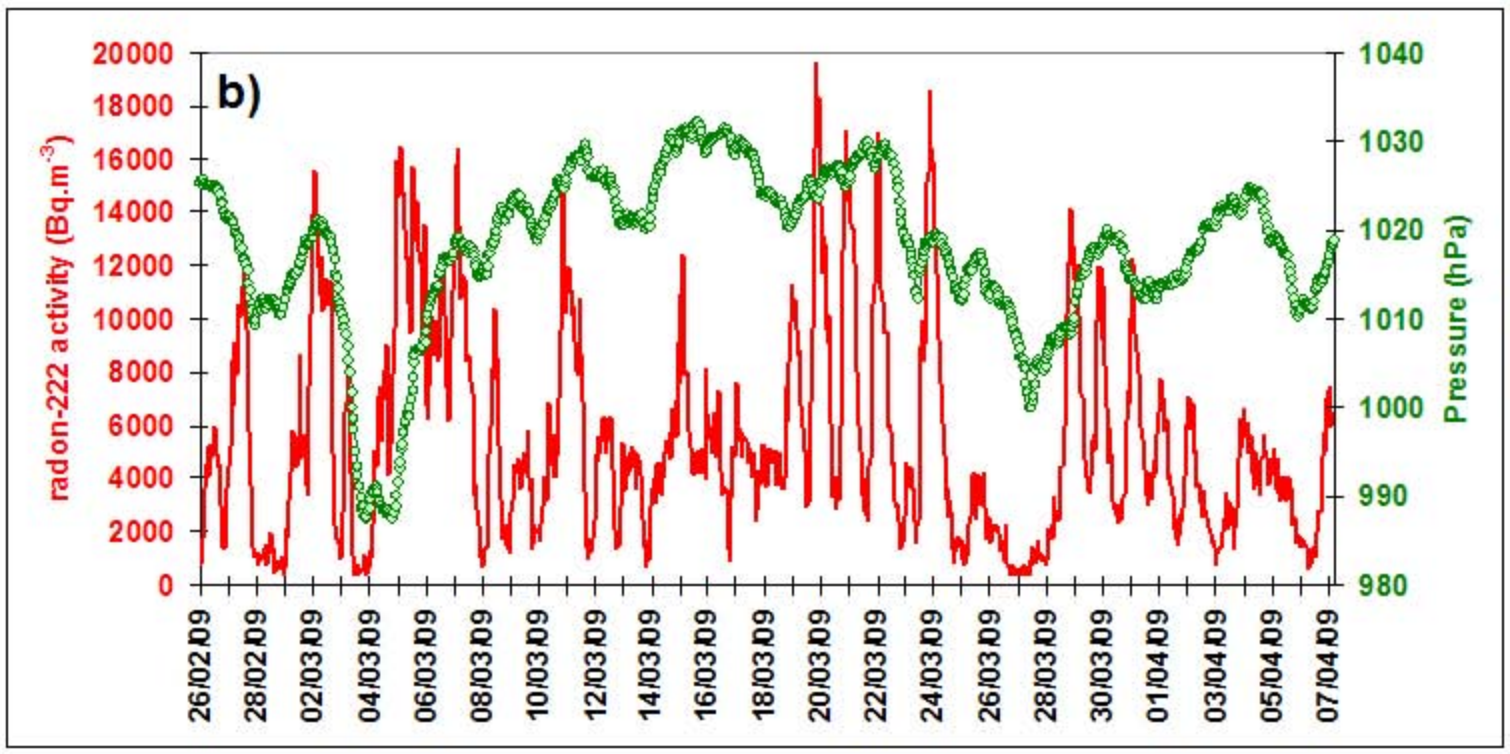
b)
radon-222 activity (Bq.m-3)
Pressure (hPa)
20000
18000
16000
14000
12000
10000
8000
6000
4000
2000
0
1040
1030
1020
1010
1000
990
980
26/02/09
28/02/09
02/03/09
04/03/09
06/03/09
08/03/09
10/03/09
12/03/09
14/03/09
16/03/09
18/03/09
20/03/09
22/03/09
24/03/09
26/03/09
28/03/09
30/03/09
01/04/09
03/04/09
05/04/09
07/04/09

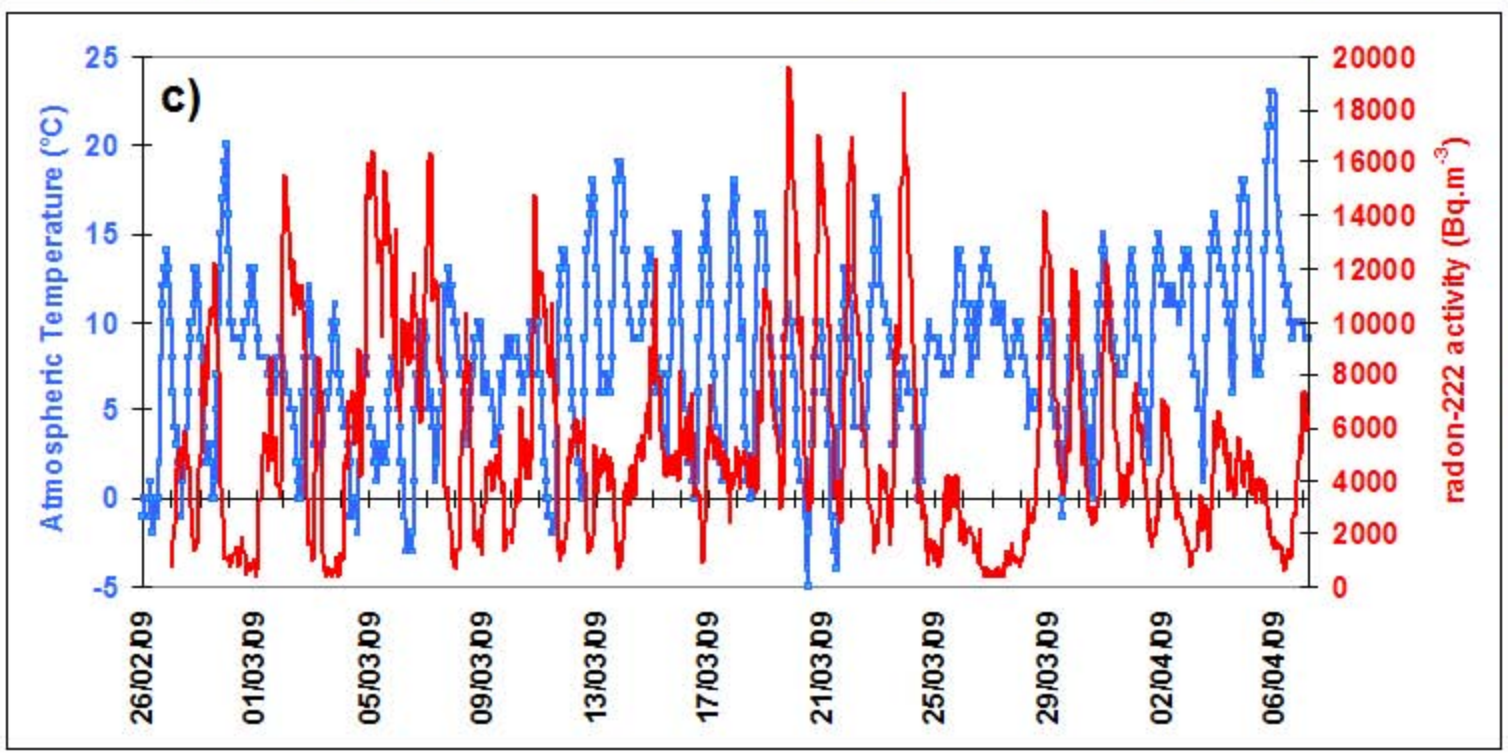
c)
Atmospheric Temperature (°C)
radon-222 activity (Bq.m-3)
25
20
15
10
5
0
-5
20000
18000
16000
14000
12000
10000
8000
6000
4000
2000
0
26/02/09
01/03/09
05/03/09
09/03/09
13/03/09
17/03/09
21/03/09
25/03/09
29/03/09
02/04/09
06/04/09

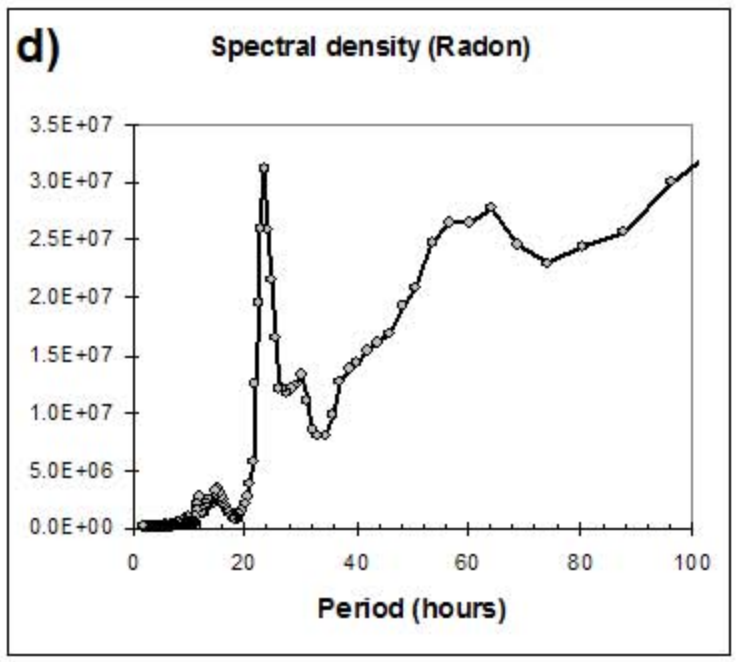
d)
Spectral density (Radon)
3.5E+07
3.0E+07
2.5E+07
2.0E+07
1.5E+07
1.0E+07
5.0E+06
0.0E+00
0
20
40
60
80
100
Period (hours)

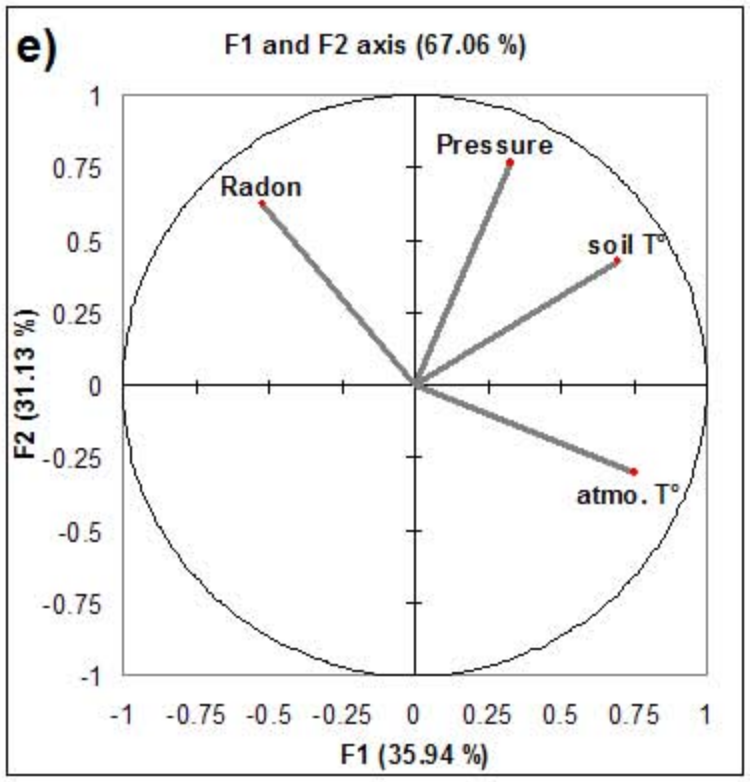
e)
F1 and F2 axis (67.06 %)
Radon
Pressure
soil T°
atmo. T°
F2 (31.13 %)
F1 (35.94 %)
1
0.75
0.5
0.25
0
-0.25
-0.5
-0.75
-1
-1
-0.75
-0.5
-0.25
0
0.25
0.5
0.75
1

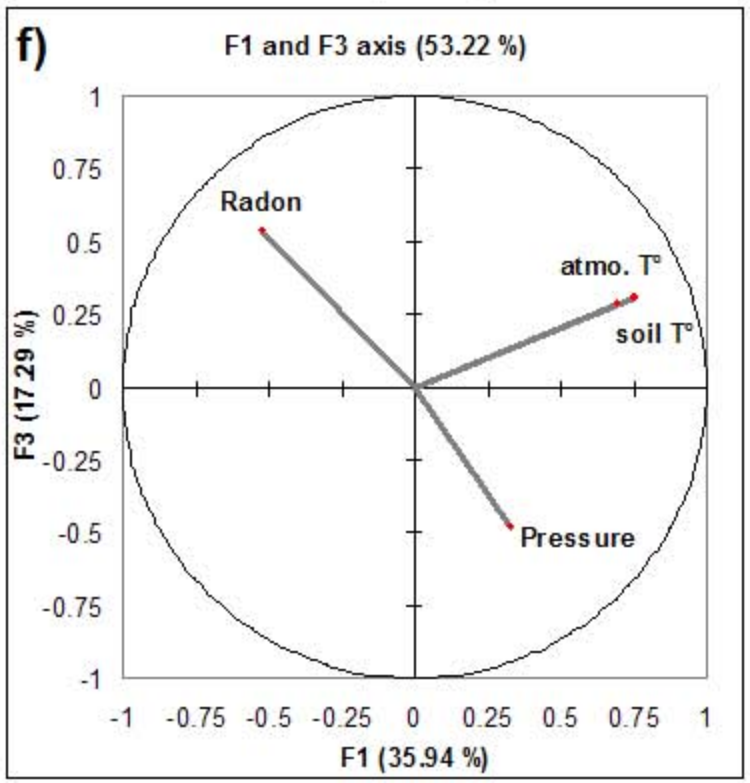
f)
F1 and F3 axis (53.22 %)
Radon
atmo. T°
soil T°
Pressure
F3 (17.29 %)
F1 (35.94 %)
1
0.75
0.5
0.25
0
-0.25
-0.5
-0.75
-1
-1
-0.75
-0.5
-0.25
0
0.25
0.5
0.75
1

a)

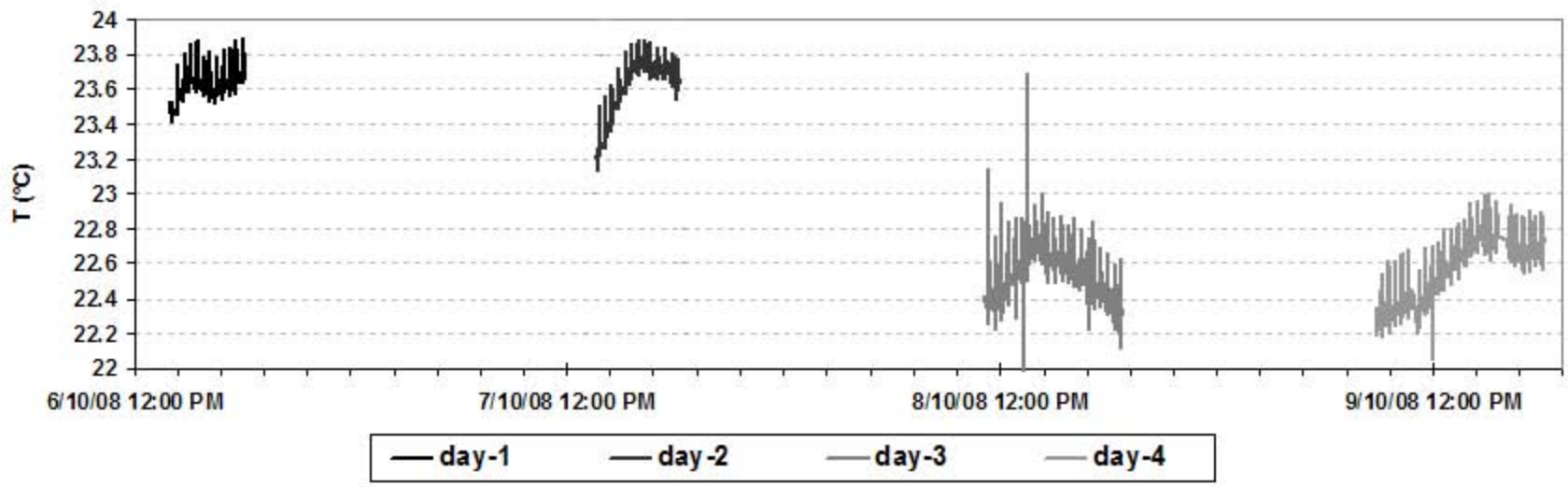
T (°C)
24
23.8
23.6
23.4
23.2
23
22.8
22.6
22.4
22.2
22
6/10/08 12:00 PM
7/10/08 12:00 PM
8/10/08 12:00 PM
9/10/08 12:00 PM
day-1
day-2
day-3
day-4

b)
day-2

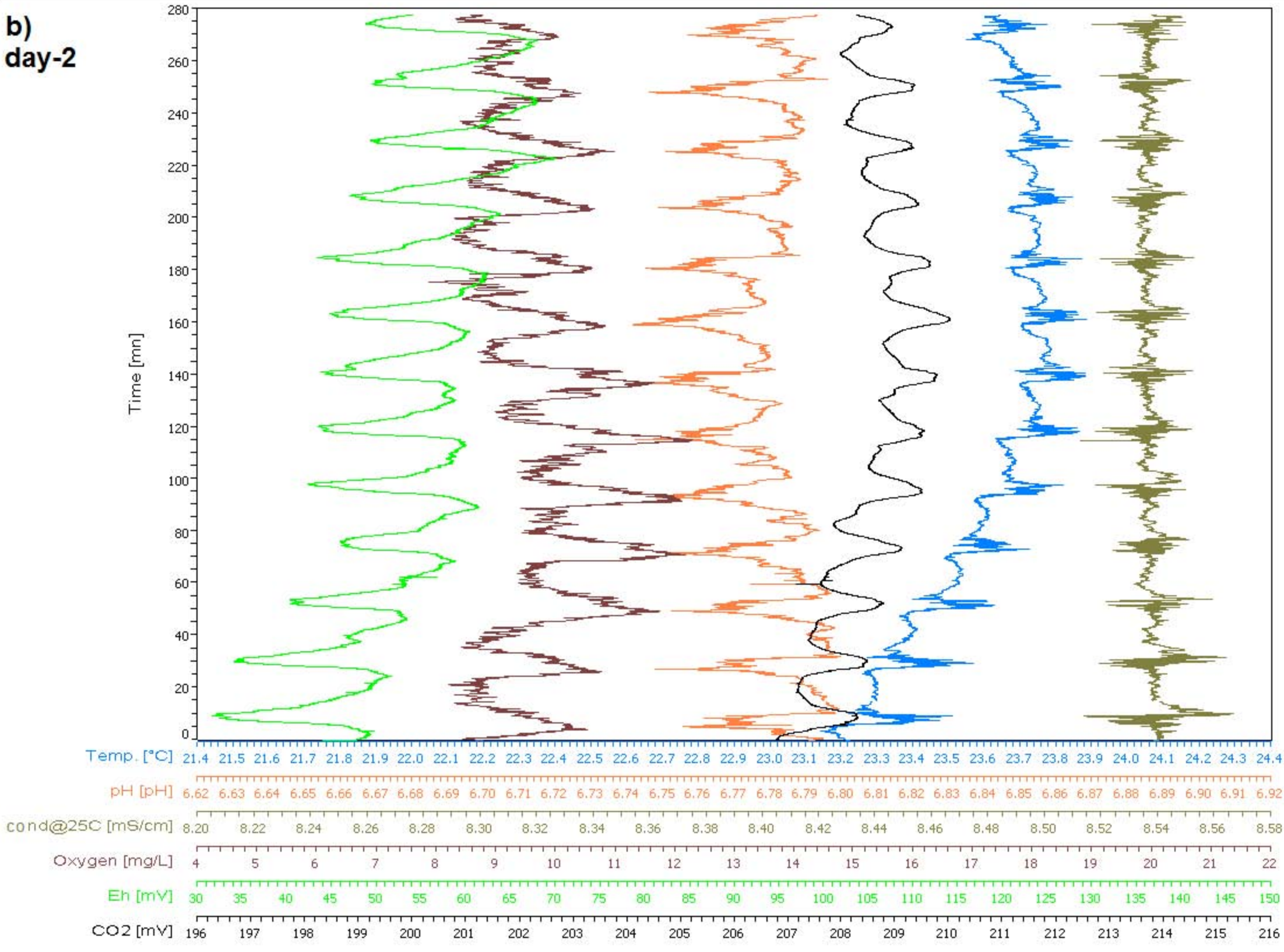
Time [mn]
280
260
240
220
200
180
160
140
120
100
80
60
40
20
0
Temp. [°C] 21.4 21.5 21.6 21.7 21.8 21.9 22.0 22.1 22.2 22.3 22.4 22.5 22.6 22.7 22.8 22.9 23.0 23.1 23.2 23.3 23.4 23.5 23.6 23.7 23.8 23.9 24.0 24.1 24.2 24.3 24.4
pH [pH] 6.62 6.63 6.64 6.65 6.66 6.67 6.68 6.69 6.70 6.71 6.72 6.73 6.74 6.75 6.76 6.77 6.78 6.79 6.80 6.81 6.82 6.83 6.84 6.85 6.86 6.87 6.88 6.89 6.90 6.91 6.92
cond@25C [mS/cm] 8.20 8.22 8.24 8.26 8.28 8.30 8.32 8.34 8.36 8.38 8.40 8.42 8.44 8.46 8.48 8.50 8.52 8.54 8.56 8.58
Oxygen [mg/L] 4 5 6 7 8 9 10 11 12 13 14 15 16 17 18 19 20 21 22
Eh [mV] 30 35 40 45 50 55 60 65 70 75 80 85 90 95 100 105 110 115 120 125 130 135 140 145 150
CO2 [mV] 196 197 198 199 200 201 202 203 204 205 206 207 208 209 210 211 212 213 214 215 216

	CO_2 (%)	CO_2 (%)	CO_2 (%)	^{222}Rn (Bq.m^{-3})	^{222}Rn (Bq.m^{-3})	^{222}Rn (Bq.m^{-3})	^{4}He (ppm)	^{4}He (ppm)	^{4}He (ppm)
	all data	**1992**	**2006-2010**	**all data**	**1992**	**2006-2010**	**all data**	**1992**	**2006-2010**
nb. of measurements	*1058*	*504*	*554*	*913*	*503*	*410*	*917*	*431*	*486*
minimum	0.05	0.08	0.05	144	148	144	< 0.05	2.58	< 0.05
maximum	100	91.40	100	2482000	1930000	2480000	17.68	17.68	9.83
1st quartile	1.40	1.18	3.31	15800	17000	13800	5.19	5.24	5.04
median value	4.64	1.70	15.76	39800	37000	43200	5.24	5.30	5.22
3rd quartile	24.08	5.10	47.00	80000	71000	97400	5.34	5.36	5.26
mean value	18.66	7.07	29.21	81700	57200	112000	5.30	5.42	5.19
standard deviation	27.23	13.48	31.90	189700	105000	250000	0.76	0.81	0.69
coeff. of variation	1.46	1.91	1.09	2.32	1.84	2.28	0.14	0.15	0.13

Sample	T (°C)	pH	cond@25°C (µS.cm^{-1})	Eh (mV)	Ca (mg/l)	Mg (mg/l)	Na (mg/l)	K (mg/l)	Fe(III) (mg/l)	Mn (mg/l)	Sr (mg/l)	Li (mg/l)	HCO_3 (mg/l)	Cl (mg/l)	SO_4 (mg/l)	PO_4 (mg/l)	NO_3 (mg/l)	F (mg/l)	Br (mg/l)	SiO_2 (mg/l)	$\delta^{18}O$ (‰ VSMOW)	δD (‰ VSMOW)	*theoretical δD if belonging to LMWL*	$^{87}Sr/^{86}Sr$	$^{13}C_{gas}$ *open sys.*
Chapelle 1 (2006)	17.8	6.54	5210	338	237	121	776	81.9			3.74		2288	717	146		4.9				-8.3	-57.4	*-53.3*	0.712298	*-4.6*
Chapelle 1 (2007)	16.6	6.63	4530	391	248	137	875	97.4			4.37	4.48	2465	806	155		2.8	0.7	1.8						*-5.1*
Chapelle 2 (2006)	18	6.21	3070	336	196	117	304	34.5			2.5		1276	298	192		6.3				-7.5	-53.7	*-46.9*	0.712818	*-2.8*
Chapelle 2 (2007)	16.6	6.33	3130	444	188	127	360	39.1			2.38	1.66	1483	340	202		4.4	0.9	0.7						*-3.4*
Chapelle 3 (2006)	17.5	6.38	2730	340	178	104	266	34.6		0.02	2.16		1410	230	198		8.3				-7.7	-54	*-48.5*	0.712035	*-3.7*
Chapelle 3 (2007)	15.9	6.51	2410	420	184	126	301	40.7			2.30	1.52	1332	315	209		4.6	1.0	0.6						*-4.5*
Tennis (2006)	29.2	6.48	7970	91	306	131	1493	163		0.10	6.37		3554	1495	101						-9.6	-63.2	*-63.7*	0.713388	*-3.9*
Tennis (2007)	29	6.46	7970	140	295	135	1486	167			6.66	8.03	3515	1348	129			0.5	3.7						*-3.9*
Tennis (2008)	28.5	6.58	8440	138	301	133	1461	163	2.75				3527	1370	111	0.4		1.1		107	-9.5	-62.8	*-62.9*		*-4.4*
Geyser Brissac (2006)	24.6	6.65	8180	186	307	133	1497	163		0.10	6.33		4135	1429	100						-9.6	-63		0.713387	*-4.9*
Geyser Brissac (2007)	23.5	6.62	7990	180	297	136	1485	167			6.88	7.99	3534	1355	126			0.4	3.7						*-4.8*
Geyser Brissac (2008)	23	6.57	8310	158	299	132	1447	162	2.80				3562	1360	111	0.5		1.1		106	-9.5	-62.7	*-62.9*		*-4.6*
Petit Saladis (2007)	21.6	6.58	8190	245	295	136	1498	168			6.29	8.13	3554	1344	125			0.5	3.5						*-4.7*
Grand Saladis (2007)	16.1	7.24	7920	386	125	139	1579	180			2.60	8.52	3124	1414	108		11.0	0.4	3.9						*-7.6*
old plant sp. (2008)	29.3	6.7	8270	140	302	133	1457	164	2.41				3147	1390	110	0.4		0.8		105	-9.5	-63	*-62.9*		*-4.9*
Valois sp. (2008)	25.3	6.45	7840	105	298	129	1461	163	2.80				3536	1370	109	0.4		1.2		106	-9.5	-62.9	*-62.9*		*-3.9*
terrace sp. (2008)	18.6	6.45	8410	197	296	131	1459	163	2.44				3566	1360	111	0.3		1.2		102	-9.6	-62.8	*-63.7*		*-4.1*
rainwater (08/10/2008)	12.4	8.45	65	273	4.2	0.9	8.3	1.2	0.03				24	6	2		1.7			0.7	-8.8	-64.7	*-57.3*		*-9.2*

radon-222 ($Bq.m^{-3}$) DATA greater than 10 $Bq.m^{-3}$ and lesser than 10^6 $Bq.m^{-3}$	POINT 2	POINT 4			
	06/10/08 → 28/01/09	**06/10/08 → 28/01/09**	**26/02/09 → 01/09/09**	**11/09/09 → 16/03/10**	***06/10/08 → 16/03/10***
nb of meas. (hours)	2728	2729	3869	740	*7338*
hours of deployment	*2735*	*2735*	*4471*	*4459*	*11665*
Min. value	60	30	50	1030	*30*
Max. value	2.69E+05	2.14E+05	9.09E+05	9.80E+05	*9.80E+05*
1st Quartile	5820	20900	2410	5890	*9640*
Median value	28500	51700	4810	7500	*16800*
3rd Quartile	102000	71500	13600	10700	*12500*
Mean value	56500	65300	28700	26300	*31300*
std. dev.	66400	57600	73600	93200	*66100*
PEAK values: nb of meas.	3	4	1		
PEAK values: Max. value	8.57E+07	7.06E+06	1.24E+06		
Cycle analysis	no cycle	7 - 10 - 22 hours 5.5 days	15 - 25 - 39 - 74 hours	24 - 58 hours	

DESCRIPTIVE	day 1 (7400 data)					day 2 (8300 data)					day 3 (13800 data)					day 4 (15800 data)				
STATISTICS	**T°**	**EC**	**O_2**	**pH**	**Eh**	**T°**	**EC**	**O_2**	**pH**	**Eh**	**T°**	**EC**	**O_2**	**pH**	**Eh**	**T°**	**EC**	**O_2**	**pH**	**Eh**
minimum	21.15	8505	7.7	6.75	1.1	23.14	8512	7.9	6.74	31.6	21.98	7621	5.3	6.40	-162.1	22.05	8477	5.9	6.43	-61.4
maximum	23.89	9184	10.8	6.80	29.7	23.88	8567	12.3	6.80	70.1	23.66	8264	18.0	7.28	206.2	23.00	8639	14.5	7.81	128.9
mean value	23.62	8532	9.2	6.78	20.5	23.62	8537	9.7	6.78	54.2	22.54	8061	9.9	6.83	69.2	22.57	8535	9.2	6.84	57.7
standard deviation	0.16	37	0.5	0.01	7.1	0.16	4	0.9	0.01	7.4	0.13	72	1.1	0.03	12.4	0.17	7	0.9	0.02	15.0